

**FLEXIBLE CERAMIC- POLYMER COMPOSITE SUBSTRATES WITH
SPATIALLY VARIABLE DIELECTRICS FOR MINIATURIZED RF
APPLICATIONS**

by

ZUHAL TASDEMIR

Submitted to the Graduate School of Engineering and Natural Sciences

in partial fulfillment of

the requirements for the degree of

Master of Science

Sabanci University

August, 2009

FLEXIBLE CERAMIC- POLYMER COMPOSITE SUBSTRATES WITH
SPATIALLY VARIABLE DIELECTRICS FOR MINIATURIZED RF
APPLICATIONS

APPROVED BY:

Asst. Prof. Gullu Kiziltas Sendur
(Thesis Supervisor)

Assoc. Prof. Mehmet Ali Gülgün

Asst. Prof. Ali Koşar

Prof. Dr. Yusuf Menceloğlu

Asst. Prof. Kürşat Şendur

DATE OF APPROVAL:

© Zuhal Tasdemir

All rights reserved

2009

To my family

ACKNOWLEDGMENTS

Firstly, I thank my supervisor Dr. Gullu Kiziltas for her inspiration and encouragement and valuable guidance in my completing this thesis. I also would like to thank my committee members, Professor Mehmet Ali Gulgun, Professor Yusuf Menciloglu, Professor Kursat Sendur and Professor Ali Kosar.

I would like to thank with all my heart to all my family, especially to my mother, my father and my little sister for their endless support and their complimentary love throughout my life.

Finally, I gratefully acknowledge the contributions of colleagues throughout this two-year journey: Gökhan Kaçar, Firuze Okyay, Cahit Dalgıçdır, Züleyha Özlem Kocabaş, Eren Şimşek, Işıl Berkün, Yasser El-Kahlout, Anasstasia Zahariouta, Emre Fırlar, Can Kartoğlu.

Flexible Ceramic- Polymer Composite Substrates with Spatially Variable Dielectrics for Miniaturized RF Applications

Zuhal TASDEMIR

MAT, Master's Thesis, 2009

Thesis Supervisor: Asst. Prof. Gullu Kiziltas

Keywords: Tape casting, dielectric properties, miniaturization, substrates, MCT dielectric ceramics

ABSTRACT

Multi-functional miniature RF devices play an important role in meeting challenging future demands within the modern communication industry. This in turn creates the need to design microwave dielectric materials with superior electrical and mechanical properties such as dielectric tunability, miniaturization, flexibility, and low loss. Although many ceramic-polymer composite substrates are presently available for RF applications, no simple manufacturing process exists today capable of producing composite substrates satisfying both high dielectric constant and low loss for miniaturization and the desired mechanical property such as flexibility for conformal applications. In order to compromise between high dielectric constant and flexibility, ceramics (MCT powders) and organic binders (polymer solution) are mixed and fabricated as films through a process called tape casting in this thesis. Prior to optimizing the process, several studies are carried out: MCT spray dried powders with $k=70$ and $k=20$ were analyzed as pressed and produced into a tape cast film. Dielectric behaviors of the samples are measured by the Agilent 16451B impedance analyzer, their microscopic behavior is examined by scanning electron microscopy. Results demonstrate that a dielectric constant 21 and 9, respectively can be achieved for non-sintered films that are deformable. Fabrication of spatially variable conformal substrates is investigated next where mosaic structures are fabricated using tape cast films and three different methods. In order to demonstrate the performance of the resulting substrates, these substrates are used to construct patch antennas and their return loss performance is measured with an Agilent Network Analyzer. For possible future design studies, antennas are also simulated using COMSOL Multiphysics 3.5a software.

**Radyo Frekansı Uygulamalarında Kullanılan Minyatürleştirilmiş Dielektrik
Özellikleri Kontrol Edilebilen Esnek Seramik Polimer Kompozit Dielektrik
Tabakalar**

Zuhal TAŞDEMİR

MAT, Master Tezi, 2009

Tez Danışmanı: Yrd. Doç. Dr. Güllü Kızıltaş

Anahtar Kelimeler: Şerit döküm, dielektrik özellikler, minyatürleştirme, tabakalar,
MCT dielektrik seramikler

ÖZET

Çok fonksiyonlu minyatür RF cihazlar, modern iletişim endüstrisinden gelecek talepleri karşılamada önemli bir rol oynar. Bu da, dielektrik özelliklerinin kontrol edilebilirliği, minyatürleştirme, esneklik ve düşük dielektrik kayıp gibi üstün elektrik ve mekanik özelliklere sahip mikrodalga dielektrik malzemelerinin tasarımını gerektirir. Her ne kadar RF uygulamalar için birçok seramik-polimer kompozit tabakalar halihazırda bulunsa da, günümüzde basit üretim süreciyle üretilmiş bükülebilirlik gerektiren uygulamalarda kullanılabilecek minyatürleştirme için gerekli olan hem yüksek dielektrik sabiti ve düşük kayıp hem de esneklik gibi istenen mekanik özelliklerin hepsini birden tatmin edebilen seramik-polimer kompozit malzeme tabakaları mevcut değildir. Bu çalışmada istenen yüksek dielektrik sabit ve esneklik özelliklerinin ikisini birden elde etmek için, seramik (MCT tozlar) ve organik bağlayıcı (polimer çözeltisi) karıştırılarak şerit döküm denilen yöntemle şerit filmler halinde üretilirler. Öncesinde süreci optimize etmek için, çeşitli çalışmalar yürütülmüştür: MCT70, MCT20 tozları hem disk hem de şerit film olarak üretilip dielektrik özellikleri incelenmiştir. Örneklerin dielektrik davranışları Agilent 16451B empedans analizörü ile, mikroskobik davranışları ise taramalı elektron mikroskobu kullanılarak karakterize edilmiştir. Elde edilen sonuçlara göre MCT70 tozundan hazırlanan kompozit filmlerin dielektrik sabiti 21, MCT20 tozundan hazırlanan kompozit filmlerin ise dielektrik sabiti 9 olarak ölçülmüştür. Diğer bir adımda ise iki boyutta değişken dielektrik özelliklere sahip bükülebilir malzeme tabakaların imalatı incelenmiştir. Mozaik yapısı denilen bu yapılar

üç yöntem kullanılarak üretilmiş ve bu mozaik tabakalar daha sonra mikroşerit anten yapımında kullanılmıştır. Anten performansları Agilent network analizörü kullanılarak ölçülmüştür. Olası tasarım çalışmalarına destek vermek ve ölçülen performansları karşılaştırmak amacı ile anten yapıları COMSOL Multiphysics 3.5a yazılımı kullanılarak simüle edilmiştir.

TABLE OF CONTENTS

ABSTRACT.....	vi
ÖZET	vii
TABLE OF CONTENTS	ix
LIST OF FIGURES.....	xi
LIST OF TABLES	xvi
1. INTRODUCTION.....	1
1.1. Motivation.....	1
1.2. Literature Review.....	2
1.3. Goals and Contributions of the Thesis	5
2. BACKGROUND	7
2.1. Background on Basic Dielectric Phenomena in Materials.....	7
2.1.1. Dielectric constant vs. capacitance	7
2.1.2. Dielectric constant in the perspective of field vectors and polarization	9
2.1.3. Frequency dependency of the dielectric constant	11
2.2. Antenna Performance: Miniaturization and Bandwidth.....	13
2.3. Magnesium Calcium Titanate (MCT) Dielectric Ceramics	14
3. EXPERIMENTAL STUDY	16
3.1. Ceramic Raw Material Characterization	17
3.2. Fabrication of Tape Cast Films via Tape Casting Process	18
3.3. Characterization of Tape Cast Films.....	20
3.4. Fabrication of Mosaic Film Substrates.....	20
3.5. Antenna Fabrication via 2D and 3D Spatially Variable Substrates using Tape Cast Films.....	24
4. CHARACTERIZATION RESULTS	28
4.1. Analysis of Dielectric Ceramic Properties	28
4.2. Analysis of Tape Cast Polymer Properties.....	32

4.3.	Analysis of Tape Cast Ceramic-Polymer Film Properties	42
4.4.	Microstructural Analysis of Ceramic Powders and Tape Cast Films	47
4.5.	Antenna Performance Measurements.....	50
4.6.	Antenna Performance Simulations.....	62
5.	CONCLUSIONS & FUTURE WORK	68
6.	BIBLIOGRAPHY	70
7.	APPENDIX.....	75

LIST OF FIGURES

Figure 2.1 A parallel-plate capacitor when a vacuum is present	8
Figure 2.2 A parallel-plate capacitor when a dielectric material is present	9
Figure 2.3 Schematic representation of an electric dipole generated by two electric charges (of magnitude q) separated by the distance d ; the associated polarization vector is depicted as P	9
Figure 2.4 (a) Imposed forces (torque) acting on a dipole by an electric field. (b) Final dipole alignment with the field	10
Figure 2.5 Dipole orientations for (a) one polarity of an alternating electric field and (b) for the reversed polarity.....	11
Figure 2.6 Variation of dielectric constant with frequency of an alternating electric field. Electronic, ionic, and orientation polarization contributions to the dielectric constant are indicated.....	12
Figure 3.1 Holes drilling process within the substrate using CNC.....	17
Figure 3.2 Ball milling process.....	19
Figure 3.3 Tape casting process.....	19
Figure 3.4 Multiple tape cast films.....	19
Figure 3.5 Resulting substrates after pressing	19
Figure 3.6 Uniaxial pressing device.....	19
Figure 3.7 Agilent 16451B impedance analyzer.....	20
Figure 3.8 Mosaic substrate made of MCT 20 and MCT 70 material	21
Figure 3.9 Mosaic substrate in Figure 3.8 in deformed state.....	21
Figure 3.10 a) 2D spatially variable flexible substrate made of MCT 20, MCT70, b) MCT15 by the dice and assembly method.	21
Figure 3.11 Machined mosaic substrates which are made from MCT70 (left), MCT20 (center) and MCT15 (right) ceramic-polymer tapes.	22
Figure 3.12 Resulting 3D spatially variable substrates after pressing three machined material layers with different dielectric constant and material layout (as shown in Figure 3.11).....	22
Figure 3.13 Drilled film with $\epsilon=15$ is mounted into another tape cast film of a) $\epsilon=20$; b) These holes are then filled with ground tape cast film of $\epsilon=70$	23

Figure 3.14 Tape cast film of $\epsilon=15$ is drilled with tip diameter of 1mm (outer rows) and 0.5 mm (inner square rows).	23
Figure 3.15 a) 2D mosaic green tape substrate and b) resulting probe fed patch antenna printed on the substrate.	24
Figure 3.16 a) Flexible substrate with patch on it and b) patch antenna with ground plane	24
Figure 3.17 a) Patch antenna on mosaic substrate in Figure 3.10 with b) flexible coaxial cable and aluminum ground plane	25
Figure 3.18 a) Patch antenna on mosaic substrate in Figure 3.12 with b) flexible coaxial cable and aluminum ground plane	25
Figure 3.19 Patch antenna on mosaic substrate shown a) in Figure 3.13 and (b) in Figure 3.14.	26
Figure 3.20 Agilent E5062A Series Network Analyzer	26
Figure 3.21 Agilent E5062A Series Network Analyzer measuring antenna in undeformed (left) and deformed states (right)	27
Figure 4.1 Dielectric constant vs. frequency (Hz) of MCT70 powder pressed pellets produced via three different processes	29
Figure 4.2 Loss tangent vs. frequency (Hz) of MCT70 powder pressed pellets produced via three different processes	30
Figure 4.3 Dielectric constant vs. frequency (Hz) of MCT20 powder pressed pellets produced via three different processes	31
Figure 4.4 Dielectric loss tangent vs. frequency of MCT20 powder pressed pellets produced via three different processes	32
Figure 4.5 ^{13}C NMR measurement of the tape cast polymer solution	33
Figure 4.6 75-MHz ^{13}C NMR spectrum of a 5% solution of PVB in Me ₂ DSO-d ₆ . The spectrum was obtained with broad-band proton decoupling at a temperature of 100 °C. ³³	34
Figure 4.7 100 MHz ^{13}C - NMR spectra of PVA in D ₂ O. ³⁴	34
Figure 4.8 FT-IR spectra of tape cast polymer solution	35
Figure 4.9 FT-IR spectra of Methyl Ethyl Ketone ³⁵	35
Figure 4.10 FT-IR spectra of Polyvinyl butyral ³⁶	36
Figure 4.11 FT-IR spectrum of Polyethylene glycol Mw. 1500 ³⁷	37
Figure 4.12 DSC thermogram of the tape cast polymer solution with isothermal steps.	38

Figure 4.13 DSC thermogram of the tape cast polymer solution from room temperature up to 450°C.	38
Figure 4.14 TGA measurement of the tape cast polymer solution from room temperature up to 450 °C.	39
Figure 4.15 EDS measurement of the dry tape cast polymer solution.....	40
Figure 4.16 Dielectric constant vs. frequency (Hz) of tape cast polymer film made of pure polymer solution.....	41
Figure 4.17 Loss tangent vs. frequency (Hz) of tape cast polymer film made of pure polymer solution.....	41
Figure 4.18 Dielectric constant vs. frequency (Hz) of MCT70 ceramic powders produced via three different processes and made into tape cast films	42
Figure 4.19 Loss tangent vs. frequency of MCT70 ceramic powder made tape cast films in four different process.....	43
Figure 4.20 Dielectric constant vs. frequency (Hz) of MCT20 ceramic powders produced via two different processes and made into tape cast films	44
Figure 4.21 Loss tangent vs. frequency of MCT20 ceramic powder made tape cast films in two different processes	45
Figure 4.22 Dielectric constant vs. frequency (Hz.) of MCT15 and magnetic ceramic powders tape cast films.....	46
Figure 4.23 Loss tangent vs. frequency of MCT15 and magnetic ceramic powder tape cast film	46
Figure 4.24 SEM image of MCT70 ceramic powder and MCT20 ceramic powder.....	47
Figure 4.25 a) SEM image of MCT20 ceramic powder as in pressed pellet from, b) post-heat treated pellet at 550°C (polymer burn-out temperature) c) pre-heat treated powder pellet at 550°C (polymer burn-out temperature) for 1 hr	48
Figure 4.26 a) MCT20 ceramic- polymer composite tape cast films as in the green state, b) as made from the heat treated powder at 550°C (polymer burn-out temperature) for 1 hr, and c) as post-heat treated tape cast film at 550°C polymer burn-out temperature) for 1 hr	49
Figure 4.27 a) SEM image of MCT70/polymer composite as it is in green state, b) tape cast film made from pre-heat treated powder at 550°C polymer burn-out temperature) for 1 hr. and c) post-heat treated tape cast film at 550°C polymer burn-out temperature) for 1hr	50
Figure 4.28 Antenna on substrate fabricated using the dice and assembly method.....	51

Figure 4.29 S_{11} (dB) vs. frequency (Hz) for the antenna made of the substrate in Figure 4.28.....	51
Figure 4.30 Antenna on substrate in Figure 3.10 fabricated using the dice and assembly method	53
Figure 4.31 S_{11} (dB) vs. frequency (Hz) response for the antenna made of the substrate in Figure 4.30 as in the undeformed state.....	54
Figure 4.32 S_{11} (dB) vs. frequency (Hz) response for the antenna made of the substrate in Figure 4.19 as in the deformed state.....	54
Figure 4.33 Antenna on substrate in Figure 3.11 fabricated using the second fabrication method	55
Figure 4.34 S_{11} (dB) vs. frequency (Hz) response of the antenna in Figure 4.33 as in the undeformed state	55
Figure 4.35 S_{11} (dB) vs. frequency (Hz) response of antenna in Figure 4.33 as in the deformed state.	56
Figure 4.36 Agilent 8720ES Network Analyzer.....	56
Figure 4.37 Antenna on substrate in Figure 3.14 fabricated using the drill and fill method	57
Figure 4.38 S_{11} (dB) vs. frequency (Hz) response of the antenna in Figure 4.37 as in the undeformed (flat) state	57
Figure 4.39 S_{11} (dB) vs. frequency (Hz) response of the antenna in Figure 4.37 as in the horizontal bended position according to feed location in the patch.....	58
Figure 4.40 S_{11} (dB) vs. frequency (Hz) response of the antenna in Figure 4.37 as in the vertical bended position according to feed location in the patch.....	58
Figure 4.41 Antenna on substrate in Figure 3.13 (b) fabricated using the drill and fill method	59
Figure 4.42 S_{11} (dB) vs. frequency (Hz) response of the antenna in Figure 4.41 as in the undeformed state	59
Figure 4.43 S_{11} (dB) vs. frequency (Hz) response of the antenna in Figure 4.41 as in the horizontal bended position.....	60
Figure 4.44 S_{11} (dB) vs. frequency (Hz) response of the antenna in Figure 4.41 as in the vertical bended position.....	60
Figure 4.45 Antenna on fabricated spatially variable substrate (size=40 mm) left and on standard FR4 substrate (right) (size=200 mm)	61

Figure 4.46 S_{11} (dB) vs. frequency (Hz) response of an antenna on a standard substrate FR4, shown in Figure 4.45 right	61
Figure 4.47 CAD Model, 3D Mesh of CAD, resulting field distribution for antenna in Figure 4.28.....	63
Figure 4.48 P1/PPort distribution simulations of antenna on substrateshown in Figure 4.28.....	63
Figure 4.49 Return loss S_{11} (dB) vs. frequency (Hz) simulations of antenna printed on substrate shown in Figure 4.28	64
Figure 4.50 CAD Model, 3D Mesh of CAD, resulting field distribution for antenna in Figure 4.30.....	65
Figure 4.51 P1/PPort distribution of the antenna on substrate in Figure 4.30.....	66
Figure 4.52 Return loss S_{11} (dB) vs. frequency (Hz) simulation result for antenna printed on substrate in Figure 4.30.....	67

LIST OF TABLES

Table 2-1 Dielectric constants and dielectric strengths for some materials¹⁷ 12

Table 4-1 Mesh statistics for the antenna simulation on the substrate shown in Figure 4.28 62

Table 4-2 Mesh statistics for the antenna simulation on the substrate shown in Figure 4.30 65

CHAPTER 1

1. INTRODUCTION

1.1. Motivation

The telecommunication industry has been expanding in the last decade or so along with the demand for miniaturized and low loss microwave devices. The high demand for making these devices smaller more integrated and cheaper automatically implies use of high dielectric constant substrates for multi-functional devices, such as broadband miniaturized antennas^{1,2}. On top of these requirements, conformability is also desired for applications where the mounting surface is not flat because antennas on conformal/pliable substrates fit easily with the curvature and contour of various geometries, such as aircrafts, missiles, and vehicles. In order to meet both the desired electromagnetic performance such as bandwidth and miniaturization coupled with good mechanical properties such as durability and flexibility, polymer- ceramic composite substrates have been intensively studied^{3,4}.

The expanding telecommunications industry has increased the demand for high dielectric constant/low loss microwave substrates applied in RF devices, such as antennas, capacitors, ultrasonic resonators, high-power transducer, actuators, and so on. Traditionally, RF (Radio Frequency) devices exploit geometry and energy feeds to maximize their performance. New strategies are exploiting 3-dimensional (3D) engineered magneto-dielectric and polymer composites to improve performance such as high efficiency and size reduction². Their realization is extremely important to the next generation of RF integrated and electronic devices such as miniaturized broadband antennas, smart sensors, and high magnetic-energy storage devices. Standard miniaturized low-loss device substrates are commonly restricted to off-the-shelf ceramics with composite forms also made available recently but these materials lack deformability so they cannot be easily and economically formed into desired complex structures for the proper microwave behavior control⁵. Specifically, for applications where the device has to be mounted on a curved base conformality also becomes a

bottleneck. However, ceramics naturally lack flexibility. Therefore, polymer-ceramic composites have been intensively studied with major work primarily focusing on their dielectric tunability and easy processing capability.

Because ceramics offer good electromagnetic properties (high dielectric constant that is needed for miniaturization) and polymers offer desired mechanical properties such as flexibility and easy manufacturing polymer-ceramic composite substrates are investigated in this thesis. In particular, three properties are of prime importance for RF applications: tunability of dielectric constants, which is achieved by spatially variable ceramic composite materials, low dielectric loss and its controllability and lastly flexibility of substrates via low temperature processing characteristics of polymers.

1.2. Literature Review

In literature, polymeric composites have been primarily studied due to their excellent properties, such as high dielectric constants and good electrical activity property, which are very useful characteristics for dielectric materials desired in capacitors, ultrasonic resonators, high-power transducer, actuators, and so on. It is well known that smart materials can be prepared by combining the excellent toughness of polymer materials with the electric activity property of ceramics. Since ceramics have a characteristic high dielectric performance and polymers have low cost and are easily processed, polymer-ceramic materials have aroused much attention for uses in microelectronics applications⁶. However, the focus in literature is mostly on one aspect of the desired characteristics of polymer-ceramic composites with no focus at all on the spatial variation of the dielectric constant as desired in many RF devices. Below examples of studies with a target falling within three categories of high dielectric constant and low-loss, tunability and processing based on tape-casting are discussed.

High dielectric constant low loss polymer ceramic composites:

For ceramic polymer composites, the highest dielectric constant is recorded as 140 for the polyvinyl butyral/lead zirconate titanates composites⁷. In this study, authors investigated the effect of frequency and polymer content to the dielectric constant by varying the polymer volume fraction and measuring the dielectric constant at various range of frequencies and various polymer volume fractions.

Another research has been done on the dielectric constant properties of the three different ceramic-epoxy composites; besides, effects of the filler ratio and testing temperature and frequency on the dielectric properties of these three composites were investigated. Its 40%-filler composite had a dielectric constant of 44, which was higher than those of 27 and 24 for the commercial BaTiO_3 and $\text{Pb}(\text{Mg}_{1/3}\text{Nb}_{2/3})\text{O}_3$ composites⁴, which is very similar to our obtained dielectric constant values, which is 19 and 21 with the ceramics MCT (Magnesium Calcium Titanates).

Some other study has been done on the epoxy-AlN ceramic composites and the effects of the content of AlN filler on the physical and dielectric properties of epoxy/AlN composites were investigated and it was found out that as the content of AlN powder in the epoxy/AlN composites increases from 5 to 40 wt%, the dielectric constant increases from 6.52 to 7.28 (measured at 1 MHz). The loss tangent of epoxy/AlN composites was slightly increased as the measured frequency increases⁸.

None of the mosaic structures were deformable, so one past research made by Kolouridis et al. focused on producing flexible ceramic- polymer (PDMS) composites. These examples show that indeed high dielectric constant and flexibility of polymers were able to deliver miniaturized filters and antenna substrates that were flexible⁹.

Tunability:

The large electrical field dependent dielectric constant can be used for tunable microwave devices, such as phase shifters, tunable oscillators, tunable filters and varactors. In such devices, it is desirable to have a high dielectric tunability over a given electric field range, a low dielectric loss. One of the studies has been done on the BZT thin films deposited on $\text{LaNiO}_3/\text{Pt}/\text{Ti}/\text{SiO}_2/\text{Si}$ substrates¹⁰. Specifically in this study, compositionally graded and homogeneous $\text{Ba}(\text{Zr}_x\text{Ti}_{1-x})\text{O}_3$ (BZT) thin films were fabricated on LaNiO_3 (LNO) buffered $\text{Pt}/\text{Ti}/\text{SiO}_2/\text{Si}$ and $\text{Pt}/\text{Ti}/\text{SiO}_2/\text{Si}$ substrates by a sol-gel deposition method, respectively. These films crystallized into a single perovskite phase. The compositionally graded thin films from BaTiO_3 to $\text{BaZr}_{0.35}\text{Ti}_{0.65}\text{O}_3$ were fabricated on LNO/ $\text{Pt}/\text{Ti}/\text{SiO}_2/\text{Si}$ substrates. The tunability behavior of compositionally graded films was analyzed in order to produce optimum effective dielectric properties.

Another research has been on the dielectric tunability of bismuth-based pyrochlore dielectric thick films on alumina substrates¹¹. Authors have fabricated metal–insulator–metal capacitors structures, employing the cubic pyrochlore $\text{Bi}_{1.5}\text{Zn}_{1.0}\text{Nb}_{1.5}\text{O}_7$ (BZN) thick films by screenprinting techniques on alumina substrates. The films displayed a dielectric constant up to 130, which is a relatively high value according to our results and the dielectric loss was reported as a value lower than 0.005 at 1 MHz. Also dielectric tunabilities of the films were compared at different temperatures as part of the same study.

Tape Cast Process:

Tape casting is a material shaping process used to make flat ceramic sheets having a thickness up to about 1 mm. The principle of the process is essentially identical to spreading plaster on a wall, icing on a cake, or painting. Thickness of the deposited layer is determined by the height of the doctor blade above the polymer sheet. Very uniform thickness can be achieved by the doctor blade process¹².

One of the recent studies in tape casting is about the tape casting of piezo ceramic/polymer composites. The aim was to obtain a flexible, low cost process for medium quantities used in ultrasonic transducers for naval sonar devices, medical diagnostic systems, and non-destructive materials testing. Tape casting being a very adaptable method to produce composites, allowed a detection of signals even with low intensity¹³.

Another study has been done on the electrical properties of multilayer ZnO varistors with water-based tape casting¹⁴. In this study, authors prepared multilayer ZnO varistors by water-based tape casting with water-soluble acrylic as binders and investigated the viscosity properties of the tape casting slurry.

Another recent study is about processing and mechanical properties of textured mullite/zirconia composites by tape casting process, which is very similar to our process in terms of the tape cast polymer solution¹⁵. In this study, they have prepared textured mullite/zirconia (ZrO_2) composites were prepared from a reactive mixture of alumina (Al_2O_3) and zircon (ZrSiO_4) powders together with acicular aluminum borate templates to nucleate and texture mullite grains in the [0 0 1]. Effect of texturing on Young's modulus and strength was investigated by fabricating samples with varying degree of

grain orientation by templated grain growth (TGG). It is found that both Young's modulus and strength increases with a better orientation control of mullite grains in the longitudinal direction. The increase in strength is attributed to the fact that pores are smaller and elongated in the texture direction resulting in smaller defect size.

1.3. Goals and Contributions of the Thesis

As evident in literature, composites of dielectrics, magnetic ceramics and polymers offer the possibility of tunability, flexibility and possibly low-loss. Also, as shown in literature they permit 2D or 3D variations of material properties in space and hence control the return loss of antennas. In this thesis, the objective is to analyze dielectric tunability of flexible substrates in 2D with a possible extension to 3D high dielectric constant materials for miniaturization purposes. This concept will be investigated using three methods by controlling spatial porosity of tape cast films. These base films, the process based on tape casting capable of producing flexible polymer-ceramic magneto-dielectric composites is proposed and analyzed. It basically involves the dispersion of ceramic powders into the polymer matrix followed by the addition of organic binders and plasticizers to increase the final product properties of green tapes, such as high strength and flexibility of tapes after casting and drying.

Specifically, in addition to their known characteristics of deformability and low-temperature processing capability, resulting substrates are analyzed targeting the following features concurrently and constitute the contributions of the thesis:

- 1) Miniaturization is obtained by maintaining high dielectric constant
- 2) Tunability is obtained by using several different materials having different dielectric constants in any desired distribution of the material substrate
- 3) Complete 2D material variations are demonstrated using 3 methods:
 - 1) Machining pores in tape cast green films to deliver spatial variation of material properties which are then stacked to result in a 2D variation
 - 2) Mosaic warm binding of square pixels, which are green tapes of multi MCT/ferrite powder systems.

3) Drilling the substrates with desired diameter holes and filling these holes with an inclusion material resulting in the desired overall dielectric constant.

c) drilling the substrates into desired diameter holes and filling these holes with the material giving the desired overall dielectric constant.

4) Flexibility is a result of the tape casting process used to manufacture thin and flat sheets of MCT/ferrite ceramic based polymers.

The combination of powerful engineered designs with the proposed fabrication technique for unique possibly low-loss flexible substrate materials will serve as a general example for a new approach: To produce a 3D arrangement of magneto-dielectric material cells according to a particular engineered design creating novel flexible material systems, useful for many other multi-functional electronic and RF devices.

CHAPTER 2

2. BACKGROUND

2.1. Background on Basic Dielectric Phenomena in Materials

Dielectrics play a very important role in the performance of electromagnetic devices. They are present in capacitors, resonators, stabilizers, and antenna substrates. The set of current ceramic dielectrics consists of a finite range of properties. New device designs are becoming increasingly aggressive in terms of the material properties required and their spatial variation in properties. Although designers and theorists can validate their designs computationally, realization of an actual design is often thwarted by nonexistent materials/properties and the lack of manufacturability¹⁶.

Dielectric materials are generally non-metallic, are electrically insulating and depict behavior of separation of electrically positive and negative charged entities on a molecular or atomic level in a nature or in a synthetic way.

2.1.1. Dielectric constant vs. capacitance:

When a voltage is applied across a capacitor, one plate becomes positively charged, the other negatively charged, with the corresponding electric field directed from the positive to the negative. The capacitance C is related to the quantity of charge stored on either plate Q by¹⁷

$$C = \frac{Q}{V} \quad (1)$$

where V is the voltage applied across the capacitor. The units of capacitance are coulombs per volt, or farads (F).

For a parallel-plate capacitor with a vacuum in the region between the plates (Figure 2.1), the capacitance may be computed from the relationship;

$$C = \epsilon_0 \frac{A}{l} \quad (2)$$

where A represents the area of the plates and l is the distance between them. The parameter ϵ_0 , called the permittivity of a vacuum, is a universal constant having the value of 8.85×10^{-12} F/m.

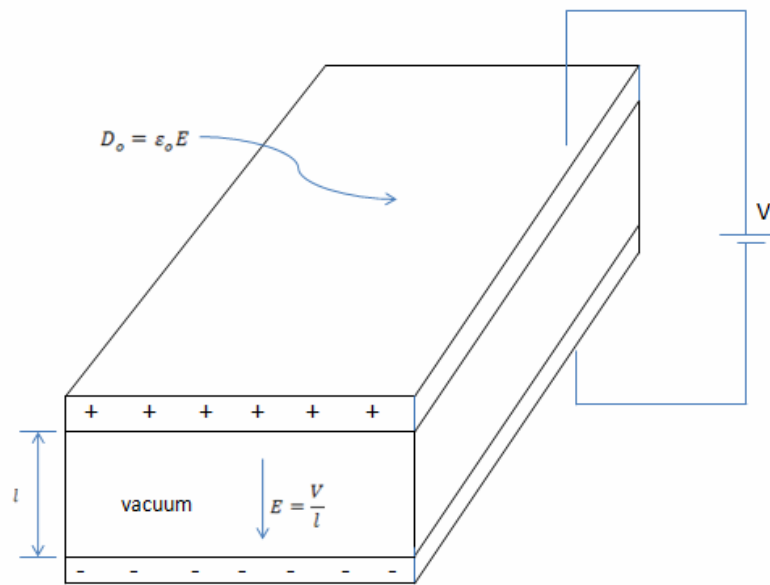


Figure 2.1 A parallel-plate capacitor when a vacuum is present

If a dielectric material is inserted into the region within the plates (Figure 2.2) then

$$C = \epsilon \frac{A}{l} \quad (3)$$

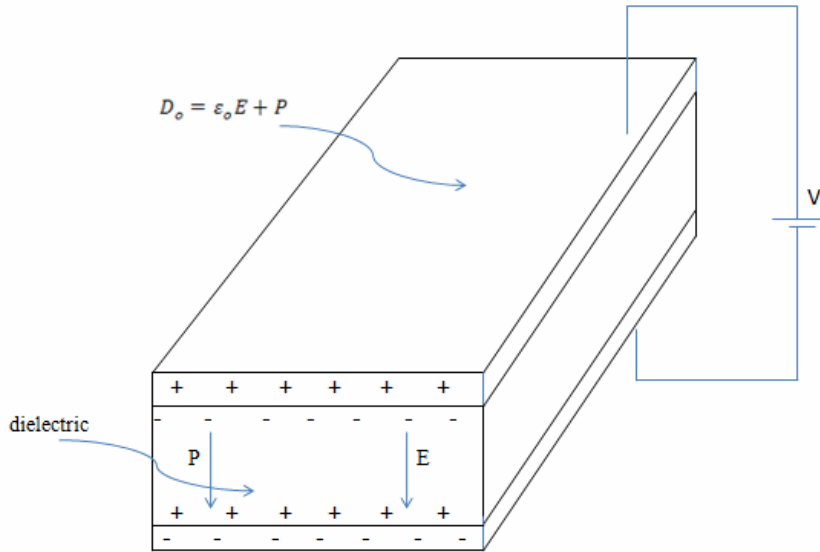


Figure 2.2 A parallel-plate capacitor when a dielectric material is present

2.1.2. Dielectric constant in the perspective of field vectors and polarization

One of the best approach for explaining the dielectric constant phenomenon is in terms of field vectors and polarization for every electric dipole there is a separation between a positive and a negative electric charge as demonstrated in Figure 2.2.

An electric dipole moment P is associated with each dipole as follows:

$$P = q.d \quad (4)$$

where q is the magnitude of each dipole charge and d is the distance of separation between them.

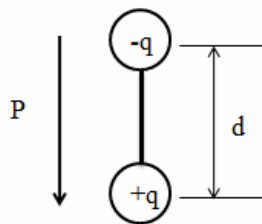


Figure 2.3 Schematic representation of an electric dipole generated by two electric charges (of magnitude q) separated by the distance d ; the associated polarization vector is depicted as P .

In reality, a dipole moment is a vector that is directed from the negative to the positive charge, as indicated in Figure 2.3. In the presence of an electric field, which is also a vector quantity, a force (or torque) will come to bear on an electric dipole to orient it with the applied field; this phenomenon is illustrated in Figure 2.4. The process of dipole alignment is termed polarization.

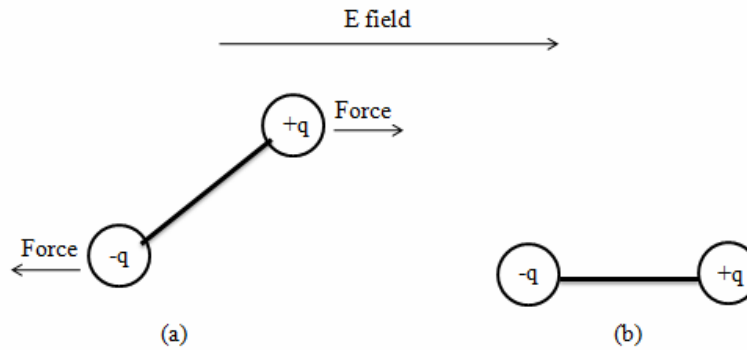


Figure 2.4 (a) Imposed forces (torque) acting on a dipole by an electric field. (b) Final dipole alignment with the field

To return to the capacitor, the surface charge density D , or quantity of charge per unit area of capacitor plate (C/m^2), is proportional to the electric field. When a vacuum is present, then

$$D_o = \epsilon_o E \quad (5)$$

the constant of proportionality being ϵ_o . Furthermore, an analogous expression exists for the dielectric case; that is,

$$D_o = \epsilon_o E \quad (6)$$

Sometimes, D is also called the dielectric displacement.

2.1.3. Frequency dependency of the dielectric constant

In many practical situations the current is alternating (ac); that is, an applied voltage or electric field changes direction with time. When a dielectric material is subjected to polarization by an ac electric field, with each direction reversal, the dipoles attempt to reorient with the field, as illustrated in Figure 2.5, in a process requiring some finite time.

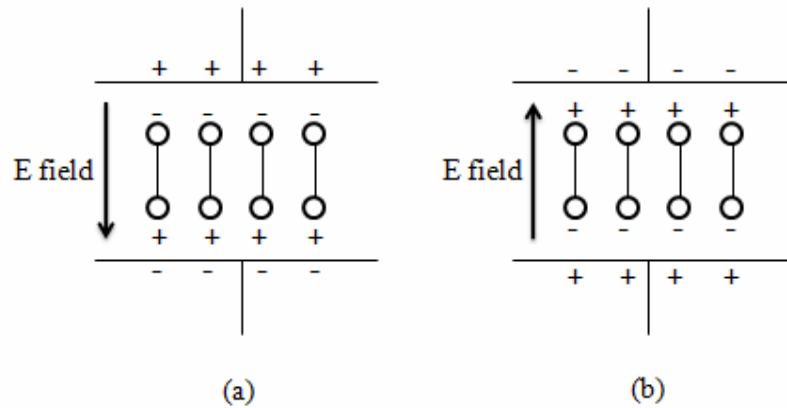


Figure 2.5 Dipole orientations for (a) one polarity of an alternating electric field and (b) for the reversed polarity

For each polarization type, some minimum reorientation time exists, which depends on the ease with which the particular dipoles are capable of realignment. A relaxation frequency is taken as the reciprocal of this minimum reorientation time. A dipole cannot keep shifting orientation direction when the frequency of the applied electric field exceeds its relaxation frequency and, therefore, will not make a contribution to the dielectric constant. The dependence of ϵ_r on the field frequency is represented schematically in Figure 2.6 for a dielectric medium that exhibits all three types of polarization; note that the frequency axis is scaled logarithmically. As indicated in Figure 2.6, when a polarization mechanism ceases to function, there is an abrupt drop in the dielectric constant; otherwise, ϵ_r is virtually frequency independent.

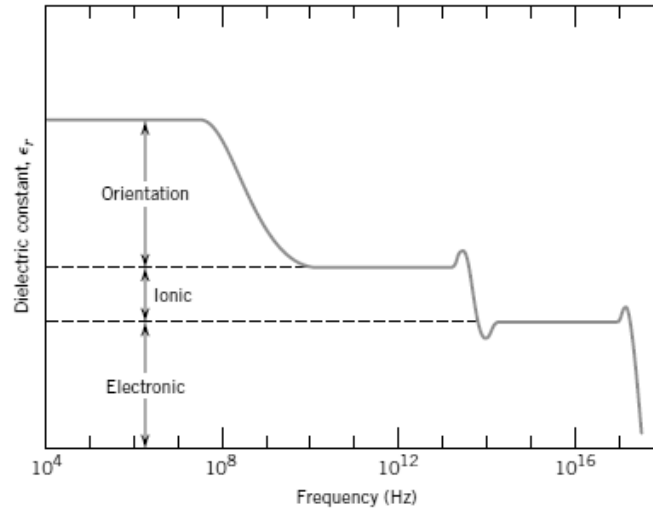


Figure 2.6 Variation of dielectric constant with frequency of an alternating electric field. Electronic, ionic, and orientation polarization contributions to the dielectric constant are indicated.

Table 2.1 presents values of the dielectric constant at 60 Hz and 1 MHz; these provide an indication of this frequency dependence at the low end of the frequency spectrum. The absorption of electrical energy by a dielectric material that is subjected to an alternating electric field is termed dielectric loss. This loss may be important at electric field frequencies in the vicinity of the relaxation frequency for each of the operative dipole types for a specific material. A low dielectric loss is desired at the frequency of utilization.

Table 2-1 Dielectric constants and dielectric strengths for some materials¹⁷

<i>Material</i>	<i>Dielectric Constant</i>		<i>Dielectric Strength</i> (V/mil) ^a
	<i>60 Hz</i>	<i>1 MHz</i>	
<i>Ceramics</i>			
Titanate ceramics	—	15–10,000	50–300
Mica	—	5.4–8.7	1000–2000
Steatite (MgO–SiO ₂)	—	5.5–7.5	200–350
Soda–lime glass	6.9	6.9	250
Porcelain	6.0	6.0	40–400
Fused silica	4.0	3.8	250
<i>Polymers</i>			
Phenol-formaldehyde	5.3	4.8	300–400
Nylon 6,6	4.0	3.6	400
Polystyrene	2.6	2.6	500–700
Polyethylene	2.3	2.3	450–500
Polytetrafluoroethylene	2.1	2.1	400–500

2.2. Antenna Performance: Miniaturization and Bandwidth

The main advantage of using high ϵ_r materials is to provide miniaturization of devices. Size reduction is of primary importance in aerospace applications where satellite communication (SATCOM) antennas may operate at 200-600 MHz. At these frequencies, the free space wavelength is on the order of 1 meter. Actual antenna size is typically quite large (0.38-0.76 m) providing a large impetus for smaller designs. Additional advantages of smaller designs include weight savings and portability. The use of dielectrics in antennas is not new. It is known that the use of high ϵ_r materials tend to reduce antenna performance via decreases in bandwidth and gain⁹. New designs are evolving that utilize high ϵ_r dielectrics that are spatially variable. Dielectric “texture” is developed by varying material properties in 3-dimensional space. Using this approach, miniaturization is achieved while maintaining performance.

Two major factors associated with radio antenna design are the antenna resonant point or centre operating frequency and the antenna bandwidth or the frequency range over which the antenna design can operate. These two factors are naturally very important features of any antenna design and as such they are mentioned in specifications for particular RF antennas. Whether the RF antenna is used for broadcasting, WLAN, cellular telecommunications, PMR or any other application, the performance of the RF antenna is paramount, and the antenna resonant frequency and the antenna bandwidth are of great importance¹⁸.

The second important antenna performance metric is the bandwidth. Most RF antenna designs are operated around the resonant point. This means that there is only a limited bandwidth over which an RF antenna design can operate efficiently. Outside this the levels of reactance rise to levels that may be too high for satisfactory operation. Other characteristics of the antenna may also be impaired away from the centre operating frequency¹⁹.

The antenna bandwidth is particularly important where radio transmitters are concerned as damage may occur to the transmitter if the antenna is operated outside its operating

range and the radio transmitter is not adequately protected. In addition to this the signal radiated by the RF antenna may be less for a number of reasons²⁰.

For receiving purposes the performance of the antenna is less critical in some respects. It can be operated outside its normal bandwidth without any fear of damage to the set. Even a random length of wire will pick up signals, and it may be possible to receive several distant stations. However for the best reception it is necessary to ensure that the performance of the RF antenna design is optimum²¹.

2.3. Magnesium Calcium Titanate (MCT) Dielectric Ceramics

Titanium Dioxide (titania) exists in 3 naturally occurring crystallographic forms: brookite, anatase, and rutile. Anatase and rutile are the phases of technological importance due to their thermodynamic stability. Rutile is the more common phase as anatase irreversibly converts to rutile around $900\pm C$. Titania is a widely used metal oxide. Its most common use is as a white pigment due to its high index of refraction.

Other applications include gas sensors, catalysts, and self cleaning coatings on windows. In single crystal form, its dielectric properties are very anisotropic. Parallel to the c-axis $k=170$ and perpendicular to the c-axis $k=85.20$ In polycrystalline sample, the relative permittivity is around 100.^{3,4} TiO_2 is technologically interesting because of its high k.

Calcium Magnesium Titanates are also of interest for microwave applications. They consist of the high k Ca-titanate and low k Mg-titanates. This occurs by a partial substitution of Mg by Ca. Compositions within the $CaTiO_3$ - $MgTiO_3$ - Mg_2TiO_4 (CT-MT- M_2T) phase system are of technological interest due to the wide range of dielectric constants available. $CaTiO_3$ (perovskite) is a high k material ($k=170$). $MgTiO_3$ (Giekielite) has a low k (17). Mg_2TiO_4 (Qandilite) also has a low k (12).

Several authors^(22, 23-29) investigated the effect of glass addition in $MgTiO_3$ - $CaTiO_3$ (MCT) ceramics. Chen et al.^{22, 23} studied the densification and microwave dielectric properties of RBS-(Mg, Ca)TiO₃, R=MgO, CaO, SrO, BaO, B=B₂O₃, S=SiO₂. The BaO-B₂O₃-SiO₂ (BBS) - ($Mg_{0.95}Ca_{0.05}$)TiO₃ (MCT) (1:1 volume ratio) composite exhibited the highest ϵ_r and quality factor. Zhang et al.²⁴ reported that Bi₂O₃-V₂O₅

addition in MgTiO_3 lowered sintering temperature from 1400°C to 875°C due to liquid-phase effect. With increasing V_2O_5 the ϵ_r decreased and the quality factor increased. This effect was attributed to the variation of the amount of different secondary phases such as $\text{Bi}_2\text{Ti}_2\text{O}_7$, $\text{Bi}_4\text{V}_{1.5}\text{Ti}_{0.5}\text{O}_{10.85}$ and BiVO_4 . At 875°C , MgTiO_3 ceramics with 5mol% Bi_2O_3 + 7mol% V_2O_5 gave excellent microwave dielectric properties such as $\epsilon_r=20.6$, $Qf=10\ 420\text{GHz}$. However, Shin et al.²⁵ found that MgTiO_3 -based dielectric decompose to MgTi_2O_5 and Mg_2TiO_4 during liquid-phase sintering using lithium borosilicate glass. However, this decomposition does not adversely affect the dielectric properties since MgTi_2O_5 has $\epsilon_r=17.4$ with $Qf=47\ 000\text{GHz}$ and Mg_2TiO_4 has $\epsilon_r=14.4$ and $Qf=55\ 000\text{GHz}$. Jantunen et al. ⁽²⁶⁻²⁹⁾ made a detailed study of the effects of different glass compositions on the tape casting and the microwave dielectric properties. They ²⁸ also investigated the sintering behavior and dielectric properties of mixtures of MMT-20 (MCT) with ZSB ($\text{ZnO-SiO}_2\text{-B}_2\text{O}_3$, 60.3:27.1:12.6) and BSB glasses ($\text{BaO-SiO}_2\text{-B}_2\text{O}_3$, 35:55:10). Jantunen et al. ²⁶ prepared LTCC by mixing 30 wt% MCT (MMT-20) ceramic powder with 70 wt% of glass-forming oxides ZnO , SiO_2 and B_2O_3 in 60.3:12.6:27.1mol%. The mixtures were ball-milled, dried and the cylindrical pucks made by sintering at 900°C . The samples prepared in this method was found to have better properties than prepared by mixing glass with ceramic powder. Hu et al. ²⁹ reported that if the $\text{MgTiO}_3\text{-CaTiO}_3$ powders contain free B_2O_3 , then tape preparation is difficult regardless of the slurry system, whereas powders containing pre-reacted B_2O_3 did not cause any problem in making dense tapes with excellent properties. Choi et al. ³⁰ reported that addition of lithium borosilicate glass to $\text{CaZrO}_3\text{-CaTiO}_3$ system lowered sintering temperature from 1450°C to 900°C . In this study we will use MCT based ceramic spray-dried powders commercially available at Transtech Inc. due to their large range of available dielectric constants (18-140) and cited low-loss behavior (loss tangents around 0.001), which were also employed earlier to produce spatially variable dielectric substrates³¹.

CHAPTER 3

3. EXPERIMENTAL STUDY

Microwave dielectric materials play an important role in designing devices with enhanced performance for a wide range of Radio Frequency applications. In order to meet the stringent needs of these systems such as conformability, low-loss and miniaturization, improved or novel microwave components based on dielectric materials and their new designs are required. The constant need for miniaturization provides a driving force for the development of existing and invention of sophisticated materials to perform the same or improved function with decreased size and weight. Dielectric materials can be either organic as in the example of polymers or inorganic like ceramics. With its wave guiding ability the choice of material directly impacts device performance because the propagation speed is indirectly proportional to the permittivity of the material, and the characteristic impedance is affected by the dielectric thickness.

There are some applications where the dielectric material is desired to have a low dielectric constant; however, miniaturized RF devices like antennas operating at low frequencies rely on the use of high dielectric constants for miniaturization. In the current study, we try to achieve a high dielectric constant by producing composite materials composed of both ceramics with high dielectric constant and deformable polymers in order to achieve both miniaturization and deformability. A high dielectric constant will essentially reduce guided wavelength so that the physical dimensions of the antenna on that substrate can be reduced as well for the same operating frequency. A high dielectric constant of the final composite is achieved by using ceramic materials, such as Mg-Ca-TiO₂ (MCT ceramics) in this study. These ceramics are mixed with polymers to obtain desired deformability of the resulting composite substrate due to polymers' low curing temperature, their ease of handling, and low cost properties. In the

present study, ceramic polymer composite films are produced via tape casting process. These films are characterized by measuring their dielectric behavior using a network analyzer and their microstructures are investigated through scanning electron microscopy. Towards the final goal of achieving monolithic conformal substrates with a dielectric spatial distribution, three methods are used for the final tunable substrates. The first one is the warm binding of substrates produced using the dice and assembly method. In this method, square pixels made of MCT green tapes are assembled resulting in 2D spatially variable mosaic substrates. The second method refers to machining of substrates via a CNC milling machine as shown in Figure 3.1. Machined substrates are then stacked onto each other resulting in 2D spatially variable mosaic substrates. The last method used refers to the drill and fill process where tape cast films were machined with 0.5 mm and 1mm diameter drill tips and resulting holes were filled with ceramic-polymer composite films ground into powder form. To test the resulting conformal substrates, a simple patch antenna was constructed using the resulting mosaic substrates of each method.



Figure 3.1 Hole drilling process within the substrate using CNC

3.1. Ceramic Raw Material Characterization:

Before producing and characterizing polymer-ceramic composite tape cast films, pellets of constituent ceramic powders were made of MCT70 and characterized to assess their dielectric constant behavior. To analyze MCT's dielectric tunability and loss controllability, pellets were produced by three different processes: 1) pressing them at 6 MPa using available spray-dried ceramic powders to understand the dielectric constant limit of the available spray dried powders; 2) heat treating the pellets produced at step 1

up to burn-out temperature at 550°C for 1 hr in order to analyze the effect of heat treatment on the dielectric constant of the ceramic pellets at the polymer burnout temperature, and 3) pre-heat treatment of the powder itself at the burnout temperature 550°C for 1hr and then pressing them into pellets at 6 MPa to analyze if the dielectric constant of ceramics increases before the tape casting process so that no additional heat treatment has to take place to increase the dielectric constant further. Sintering to higher temperatures is avoided in order to maintain the flexibility of the ceramic polymer composite films.

3.2. Fabrication of Tape Cast Films via Tape Casting Process:

A ceramic tape casting slurry based on magnesium-calcium-titanate (MCT70) was prepared. In the first step the MCT powder, the polymer solution composed of organic solvents, binder and the dispersant were ball-milled with zirconia balls (76% polymer solution, 24% MCT70 powder) for 12 h at 175 rpm speed to obtain a uniform mixture (Figure 3.2). After degassing the slurry in the magnetic stirrer for 5 hours, the slurry was cast on the glass layer to form a 130 μ - thick ceramic layer using doctor blade process (Figure 3.3). Multiple cast films (Figure 3.4) are then stacked onto each other, as shown in Figure 3.5 and pressed uniaxially (Figure 3.6) at 9 MPa to obtain a laminar structure shown in Figure 3.5.



Figure 3.2 Ball milling process



Figure 3.3 Tape casting process

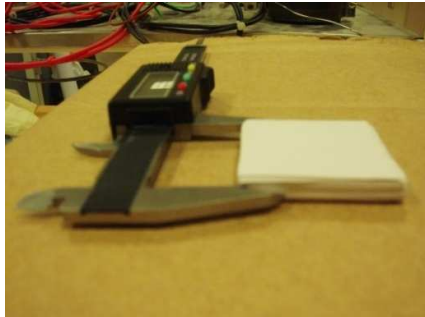


Figure 3.4 Multiple tape cast films

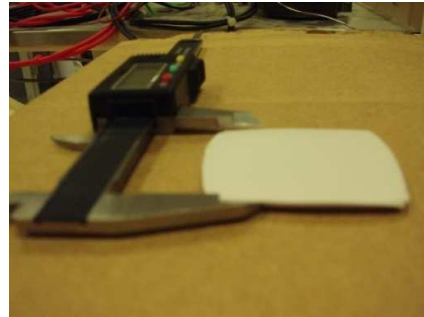


Figure 3.5 Resulting substrates after pressing

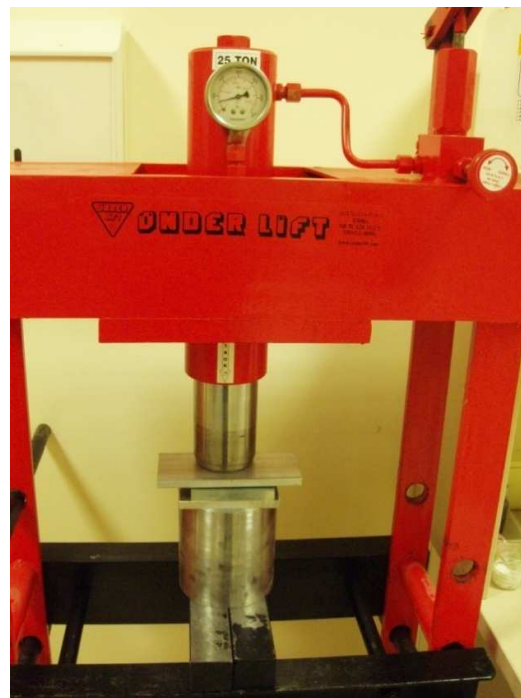


Figure 3.6 Uniaxial pressing device

3.3. Characterization of Tape Cast Films:

Knowing the dielectric constant and loss limitation of the constituent ceramic powder as explained in Section 3.1. and the effect of pre- heat treatment on the powder pressed pellets, similar analysis was made for tape cast films made from 1) as-is powders, 2) pre-heat treated powders at 550°C (polymer burn-out temperature) and 3) pre-sintered powders at 1360°C tape cast after ball-milling (uniform) or pounding in a mortar (non-uniform).

Dielectric constant and dielectric loss measurements were carried out using the Agilent 16451B Material Analysis kit with the 4294A network analyzer (Figure 3.7) between frequencies 40 Hz- 30 MHz using the specific electrode B with a diameter of 5mm.



Figure 3.7 Agilent 16451B impedance analyzer

3.4. Fabrication of Mosaic Film Substrates:

After producing ceramic polymer tape cast films, the next step was to fabricate the spatially variable conformal substrates using these films. Three different methods have been used for this goal. The first method is the “dice and assembly” method. In this method, a simple mosaic substrate as depicted in Figure 3.8 is produced via two shades of polymer tapes, namely MCT 20 and MCT 70,-via machining and assembly. Resulting layout is pressed at 3 MPa to form the conformal substrate as shown in Figure 3.9 of a patch antenna to be tested for miniaturization purposes.



Figure 3.8 Mosaic substrate made of MCT 20 and MCT 70 material

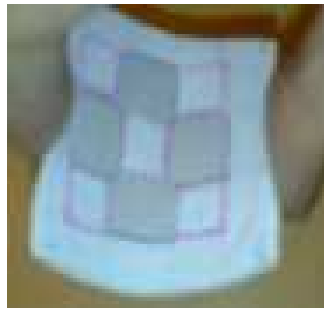


Figure 3.9 Mosaic substrate in Figure 3.8 in deformed state

With the help of the dice and assembly method, a more complex mosaic substrate with 2D material variation is produced using the same three base materials with dielectric constants of MCT 70, MCT20 and MCT15. The resulting 2D spatially variable conformal substrate is shown in its undeformed state and deformed state in Figure 3.10 (a) and (b), respectively.



Figure 3.10 a) 2D spatially variable flexible substrate made of MCT 20, MCT70, b) MCT15 by the dice and assembly method.

The second method used for fabrication of spatially variable conformal substrates refers to stacking layers of tape cast films that were machined to desired 2D material distribution as shown in Figure 3.11 to obtain the final mosaic substrate shown in Figure 3.12. In this type of fabrication, conformal substrates are made using three different dielectric constant materials: MCT20, MCT70, and MCT15. Each layer is machined into desired configuration as dictated by the design using a 1 mm drill tip with 0.5 mm radius curvature. The resulting three layers are pressed on top of each other with a pressure of 6 MPa in order to achieve the final material variation in the substrate.



Figure 3.11 Machined mosaic substrates which are made from MCT70 (left), MCT20 (center) and MCT15 (right) ceramic-polymer tapes.

In addition to the dice and assembly method, via this technique substrates made from stacking 2D tape cast films on top of each other have the potential to deliver 3D spatially variable substrates.



Figure 3.12 Resulting 3D spatially variable substrates after pressing three machined material layers with different dielectric constant and material layout (as shown in Figure 3.11)

Finally, the third method is capable of delivering 2D spatially variable substrates via the ‘drill and fill’ process. As can be seen in Figure 3.13 (a) and (b), tape cast film made from ceramic powder having a dielectric constant of 15 were drilled with a drill tip diameter of 1 mm using a CNC milling machine. These drilled square pixels are then cut from the $\epsilon=15$ film and assembled into the $\epsilon=20$ film as shown in Figure 3.13 (a). These air holes are filled with tape cast materials of $\epsilon=70$ which are grinded into powder form to increase the dielectric constant of the overall resulting substrate as depicted in Figure 3.13 (b).

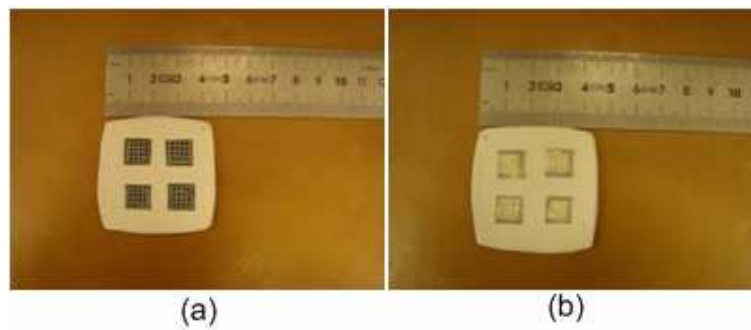


Figure 3.13 Drilled film with $\epsilon=15$ is mounted into another tape cast film of a) $\epsilon=20$; b) These holes are then filled with ground tape cast film of $\epsilon=70$.

Another substrate is fabricated from the tape cast film of $\epsilon=15$. As can be seen from Figure 3.14., the outer perimeter of the substrate is drilled with a drill tip diameter of 1 mm in the form of two rows via CNC drilling machine. The internal part of the perimeter is drilled with a drill tip diameter of 0.5 mm. Resulting holes are left empty with air of $\epsilon=1$

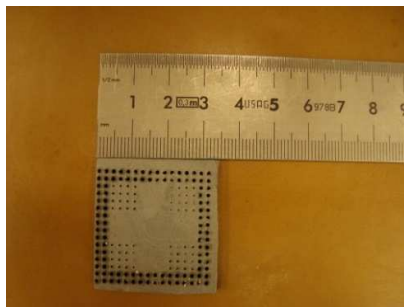


Figure 3.14 Tape cast film of $\epsilon=15$ is drilled with tip diameter of 1mm (outer rows) and 0.5 mm (inner square rows)

3.5. Antenna Fabrication via 2D and 3D Spatially Variable Substrates using Tape Cast Films

After producing flexible substrates using ceramic-polymer tape cast films with spatial variation, the next step was to test their performance as antenna substrates. Therefore, to produce the radiating antenna, copper tape was mounted on resulting substrates such as the 2D mosaic green tape produced using two shades in Figure 3.15 (a) to produce the patch antenna as shown in Figure 3.15 (b). Patch antenna was fed by a coaxial cable and a ground plane was used at the back surface of the substrate to complete the antenna. Measurements were carried out both in undeformed and deformed states (as shown in Figure 3.15 and Figure 3.16) using the Agilent E8362B PNA network analyzer.

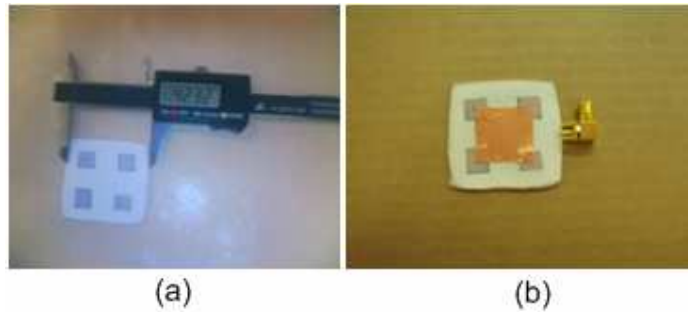


Figure 3.15 a) 2D mosaic green tape substrate and b) resulting probe fed patch antenna printed on the substrate

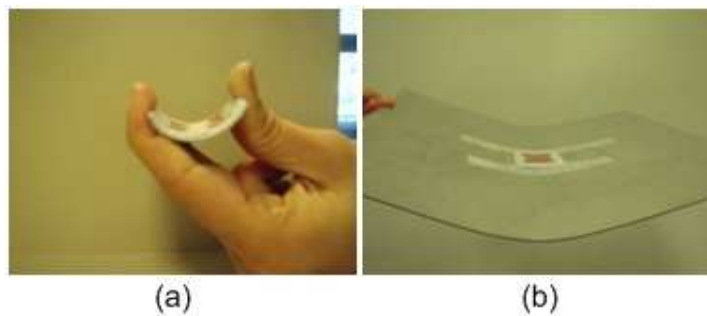


Figure 3.16 a) Flexible substrate with patch on it and b) patch antenna with ground plane

The second antenna measurement was carried out using the substrates in Figure 3.10. As can be seen from Figure 3.17, copper patch is mounted onto the substrate at the back surface of which the aluminum ground plane was attached. Feeding was achieved via a flexible coaxial cable as seen in the backview of the antenna in Figure 3.17 (b).

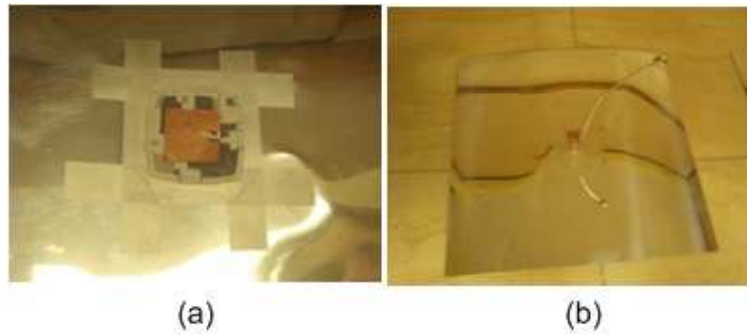


Figure 3.17 (a) Patch antenna on mosaic substrate in Figure 3.10 with (b) flexible coaxial cable and aluminum ground plane

The same procedure is also applied to the substrates in Figures 3.12, 3.13 (b), and 3.14. as can be seen from Figures 3.18, 3.19 a) and b).



Figure 3.18 a) Patch antenna on mosaic substrate in Figure 3.12 with b) flexible coaxial cable and aluminum ground plane

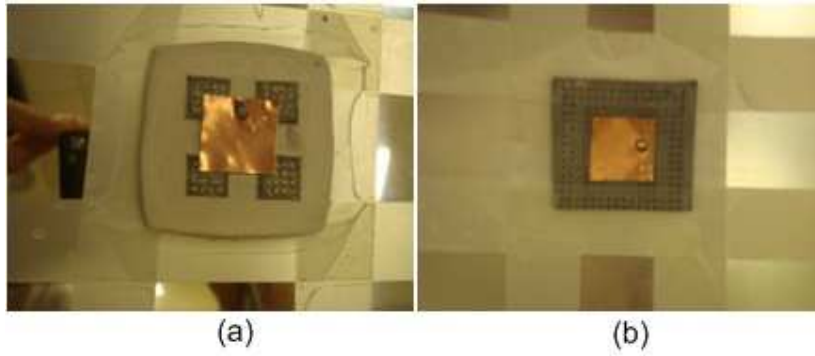


Figure 3.19 Patch antenna on mosaic substrate shown a) in Figure 3.13 b) and b) in Figure 3.14

These substrates were then measured with the Agilent E5062A Series Network Analyzer as shown in Figure 3.20 in the frequency range from 300 KHz to 3 GHz.



Figure 3.20 Agilent E5062A Series Network Analyzer

Antenna performance measurements are carried out for both the undeformed and deformed states as shown in Figures 3.21.

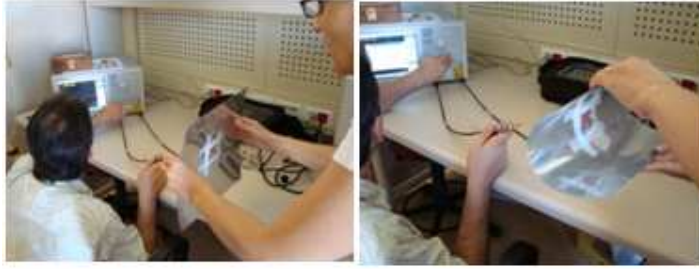


Figure 3.21 Agilent E5062A Series Network Analyzer measuring antenna in undeformed (left) and deformed states (right)

CHAPTER 4

4. CHARACTERIZATION RESULTS

In this chapter, measurement and characterization results are presented for the following four groups of materials produced and discussed in Chapter 3: Dielectric ceramics, tape cast polymer, tape cast ceramic-polymer films and antennas made of mosaic substrates. For characterization purposes, measurements comprise of dielectric measurements, scanning electron microscopy, and extensive polymer analysis including NMR FT-IR, TGA, DSC and EDS in addition to antenna measurements and simulations.

4.1. Analysis of Dielectric Ceramic Properties

In order to understand the general dielectric behavior of the dielectric powders used in the tape cast process, dielectric measurements are carried out using the Agilent 16451B Impedance Analyzer. Dielectric measurements results are presented as a function of frequency for pellets made of two basic constituents, namely MCT 70 and MCT20 dielectric powders using three different processes: firstly as pure ceramic powder pressed into pellet form, in the pellet form made from ceramic powders which are heat treated at the polymer burnout temperature 550°C, and finally pellets which are heat treated at the polymer burnout temperature 550°C. MCT15 ceramic powders cannot be measured with the material impedance analyzer which uses the capacitance method, because the pellets from the MCT15 powder are too brittle such that samples cannot be held between the conductive plates of the material impedance analyzer.

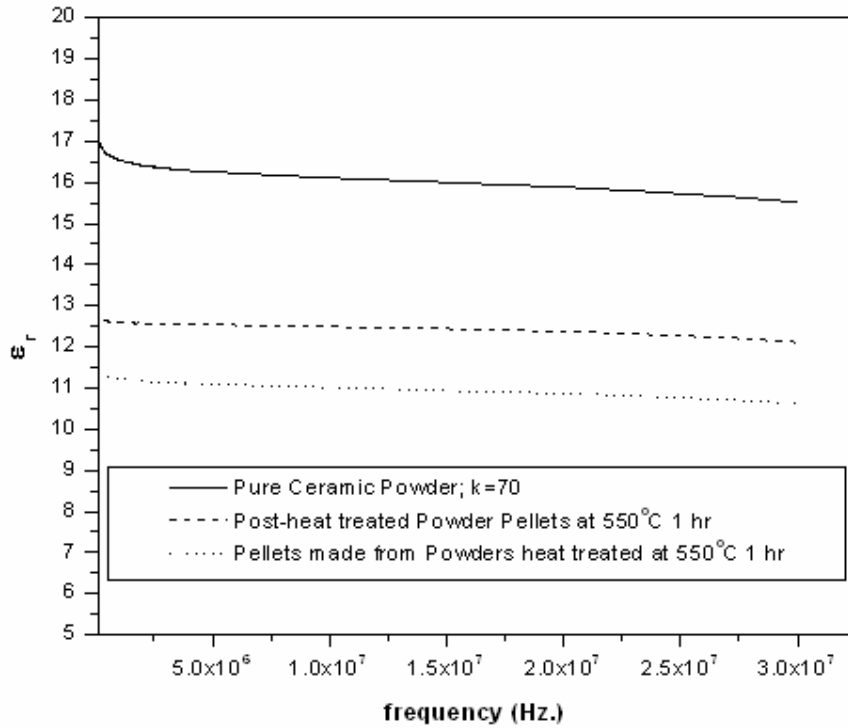


Figure 4.1 Dielectric constant vs. frequency (Hz) of MCT70 powder pressed pellets produced via three different processes

According to the measurements for MCT 70 powder shown in Figure 4.1, it is observed that the highest dielectric constant, $\epsilon \sim 16.5$ corresponds to pellets made from available spray-dried powder. This is attributed to the burn-out temperature of 550°C not being the actual full dense sintering temperature of the MCT ceramic pellets, i.e. they are only partially dense, hence a porous microstructure results in lower dielectric constant. However, powders were not fully sintered to 1360°C and heat treatments at higher temperatures were avoided to maintain flexibility of resulting films. Also, post-heat treated ceramic pellets indicate a slightly higher dielectric constant than pellets produced via pre-heat treated ceramic powders due to higher ceramic density.

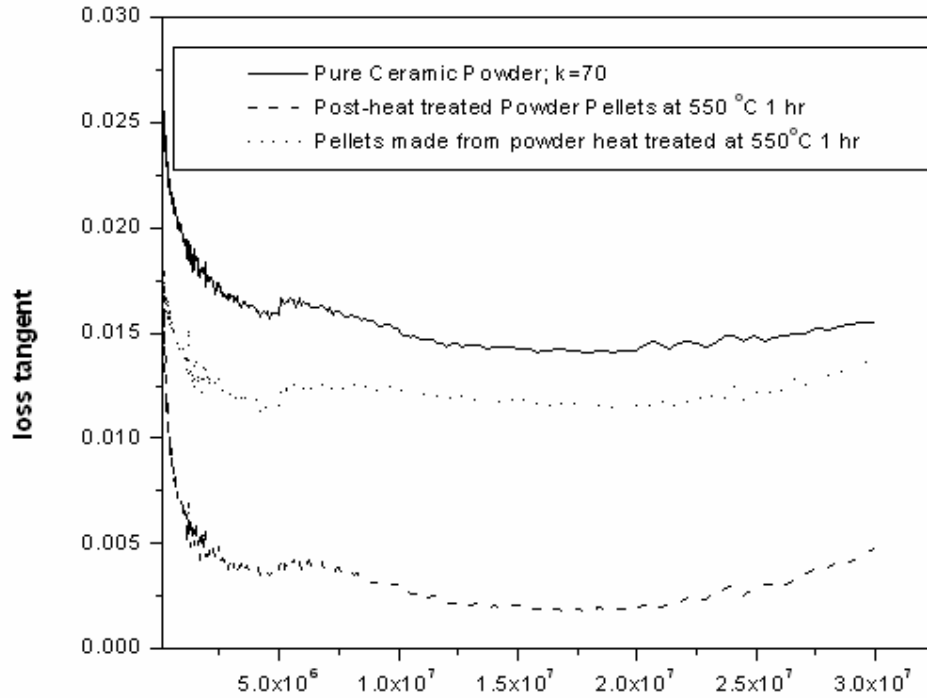


Figure 4.2 Loss tangent vs. frequency (Hz) of MCT70 powder pressed pellets produced via three different processes

In Figure 4.2, dielectric loss tangent measurements of the same pellets are given. The lowest possible dielectric loss value is achieved for sintered ceramic pellets, around a value of ~ 0.0025 . This is attributed to the fact that the amount of pores decreases during the firing process, as a result, loss value decreases. Also, loss behavior of ceramic pellets improves slightly via pre-heat treating of powders from 0.016 to 0.012.

Same dielectric constant and loss tangent measurements are performed on the MCT20 powder pellets. Referring to Figure 4.3., dielectric constant of the powder pellets made of spray dried powder is on the order of $\epsilon \sim 9$, whereas post-heat treated powder pellet has a dielectric constant of $\epsilon \sim 8$ and pre-heat treated powder pellet has a dielectric constant of $\epsilon \sim 7$. The higher dielectric constant of the pellets made of spray-dried powder than the post heat treated and pre-heat treated powder pellets can be explained similarly as in the case of the MCT70 powders. Without heat treatment ceramic powders are denser and as a result their dielectric constant is relatively high (although in the case of MCT 20 they show a low dielectric value very close to each other) in these samples. However, when heat treatment takes place, air is coming into play since air has

relatively low dielectric constant, i.e. ~ 1 . For example, in the post heat treated powder pellets, the effect of air induced by the process of sintering after the powders are pressed into pellets is obviously seen by the fact that particle size increases when heat treatment occurs. As for the pre heat treatment case, which displays the lowest dielectric constant, the effect of heat treatment on obtaining the low dielectric constant is higher since while heat treatment, moisture between the ceramic powder particles and some other compounds used in the spray dry process of ceramic powder particles is evaporated. In addition to the air resulting from the evaporation of moisture and other relatively low evaporation point products, there are also air gaps resulting from the size increase of particles during heat treatment. While pressing, the air gaps are not fully minimized and as a result of that dielectric constant decreases since it basically displays also the low dielectric constant of air.

As for the loss tangent properties of the samples made of MCT20 shown in Figure 4.4, similar trend as in the case of the MCT70 dielectric ceramic powders is observed. Dielectric loss values are on the order of 0.003 for the pure ceramic powder pellets, however, as heat treatment takes place loss tangent values are seen to drop down to 0.001 -0.002.

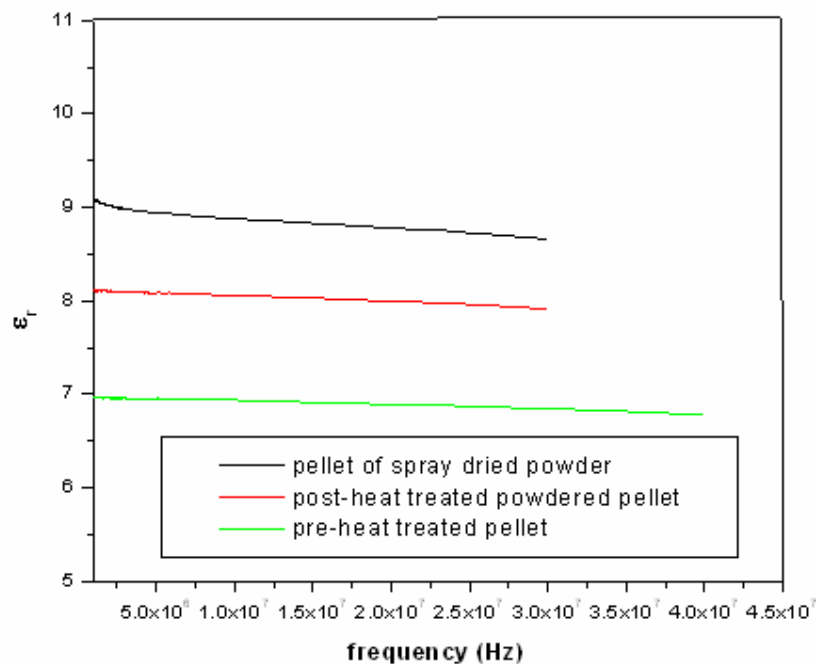


Figure 4.3 Dielectric constant vs. frequency (Hz) of MCT20 powder pressed pellets produced via three different processes

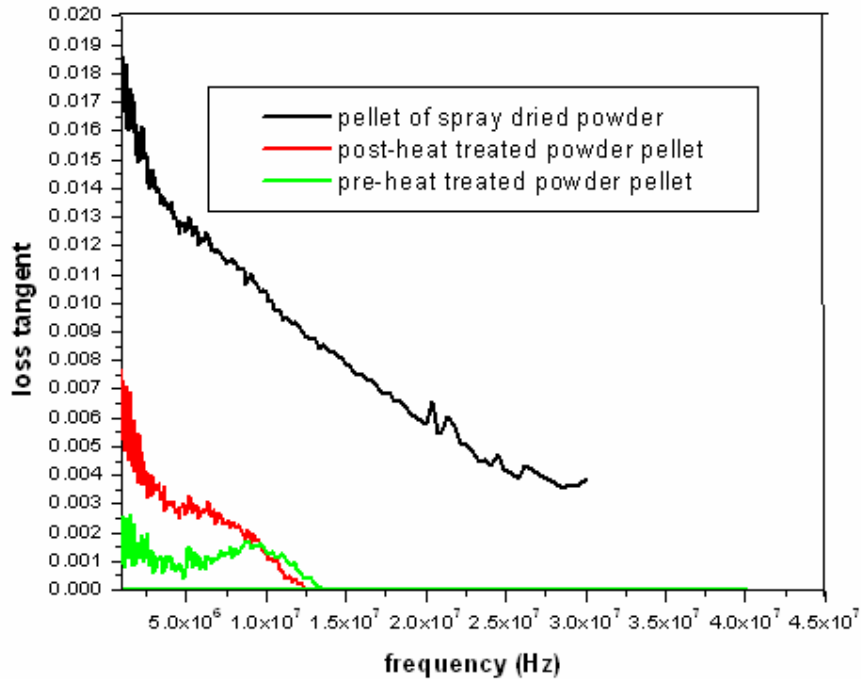


Figure 4.4 Dielectric loss tangent vs. frequency of MCT20 powder pressed pellets produced via three different processes

4.2. Analysis of Tape Cast Polymer Properties:

For the production of flexible substrates, tape cast films were produced using a polymer based solution and different spray dried ceramic constituents. Within the tape cast process, in order to obtain a homogenous tape cast slurry, a mixture of binders, dispersants and plasticizers which are found in solvents of methyl ethyl ketone/ethanol based polymer solution was used. This tape cast polymer solution was not synthesized in-house but was purchased from the MSE Tech. Co. and is listed as the product “TC-S1 Binder Organic Solution”.

The primary objective of the characterization of the tape cast solution is to identify the binder and dispersant chemicals so that these ingredients can be modified in the future to be able to tune and control the resulting tape cast film properties such as dielectric constant, loss, and uniformity according to the type of the different ceramic materials used in the tape cast process.

Therefore, the organic polymer solution is characterized focusing primarily on its composition with an initial estimation that the solution mainly consists of two standard

constituents such as PVB (poly vinyl butyral) and PEG (poly ethylene glycol). Each of these ingredients has a primary role within the slurry. Majority of the organics are in single phase, where the solvent provides the base strength, the dispersant helps deagglomerate ceramics, and the plasticizer improves flexibility and lamination³².

In order to analyze the solution composition, some characterization measurements were carried out including NMR, FT-IR, TGA, DSC and EDS characterizations followed by the dielectric measurement of the polymer solution. The NMR measurement in Figure 4.5 shows that peaks at 10, 40, 70 and 100 ppm refer to the Polyvinyl butyral, as these values are in agreement with its published NMR spectrum shown in Figure 4.6.³³

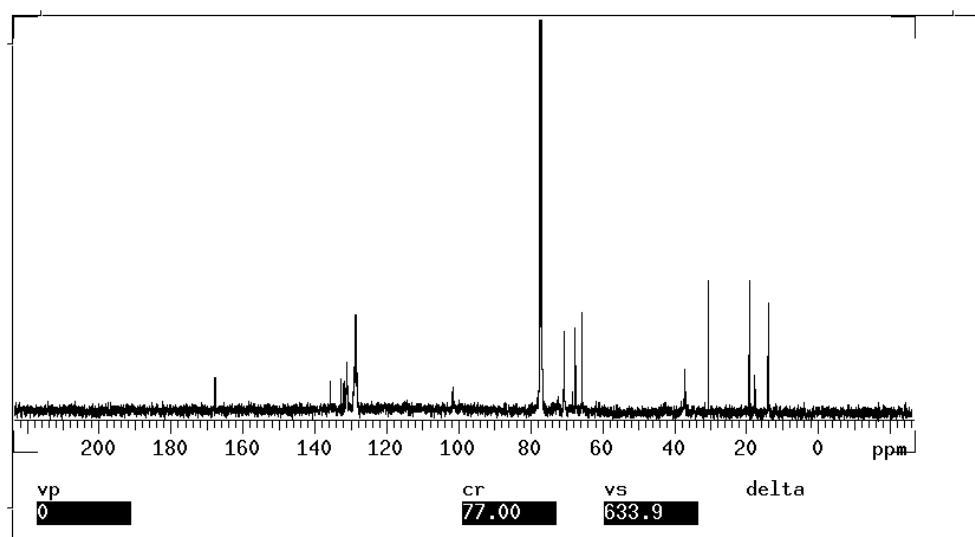


Figure 4.5 ¹³C NMR measurement of the tape cast polymer solution

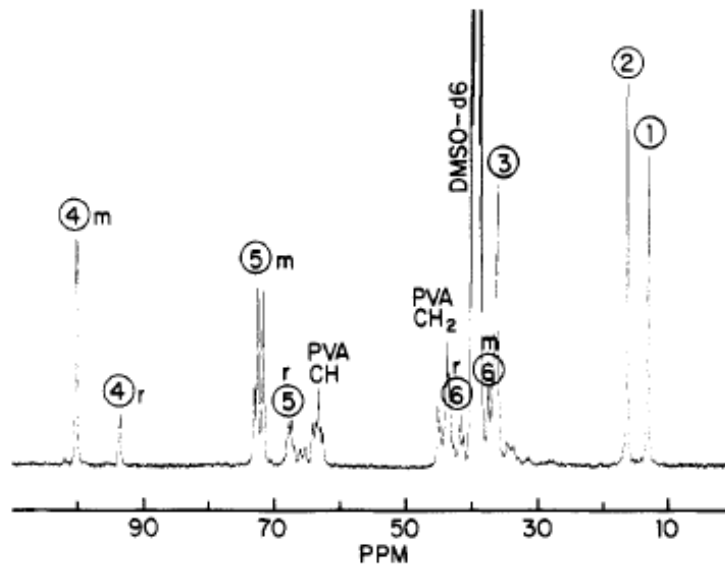


Figure 4.6 75-MHz ^{13}C NMR spectrum of a 5% solution of PVB in $\text{Me}_2\text{DSO-d}_6$. The spectrum was obtained with broad-band proton decoupling at a temperature of 100°C .³³

Considering NMR spectra results of Figure 4.7., which shows the ^{13}C -NMR spectrum of PVA, peaks around 65 ppm are consistent with the existence of Polyvinyl alcohol (PVA), which is very similar to the Poly vinyl glycol according to resonance structure in the NMR spectra.

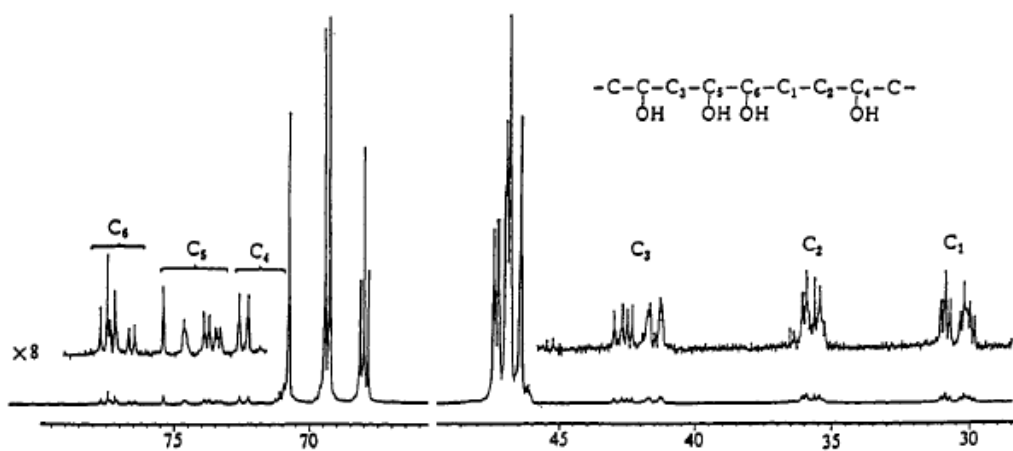


Figure 4.7 100 MHz ^{13}C - NMR spectra of PVA in D_2O .³⁴

As for the FT-IR measurement shown in Figure 4.8., when compared to the existing FT-IR spectrum of the methyl ethyl ketone³⁵ shown in Figure 4.9., similar peaks are observed around 1200, 1400 and 1700 cm^{-1} .

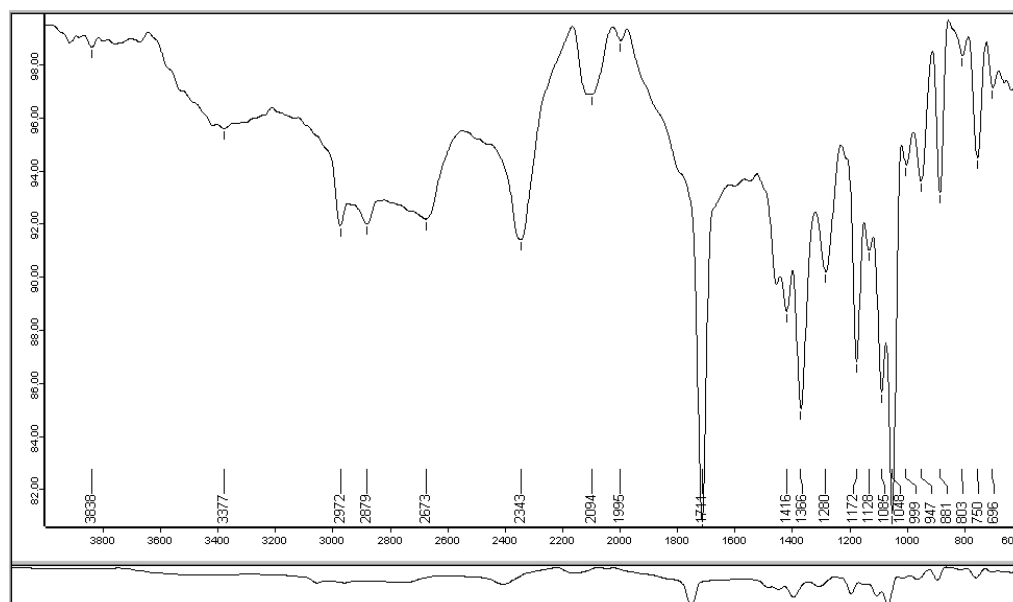


Figure 4.8 FT-IR spectra of tape cast polymer solution

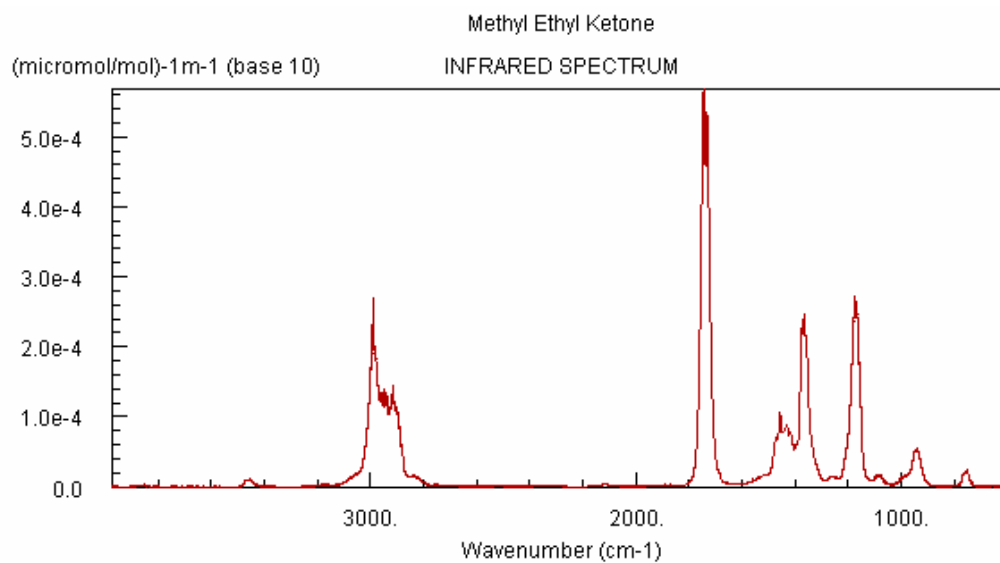


Figure 4.9 FT-IR spectra of Methyl Ethyl Ketone³⁵

In Figure 4.10, FT-IR spectrum of Polyvinyl butyral can be seen. When compared with the FT-IR measurement of the tape cast polymer solution in Figure 4.8, common peaks around 3000 cm^{-1} , 2000 cm^{-1} are observed proving that these peaks in the tape cast polymer sample belong to Polyvinyl butyral.

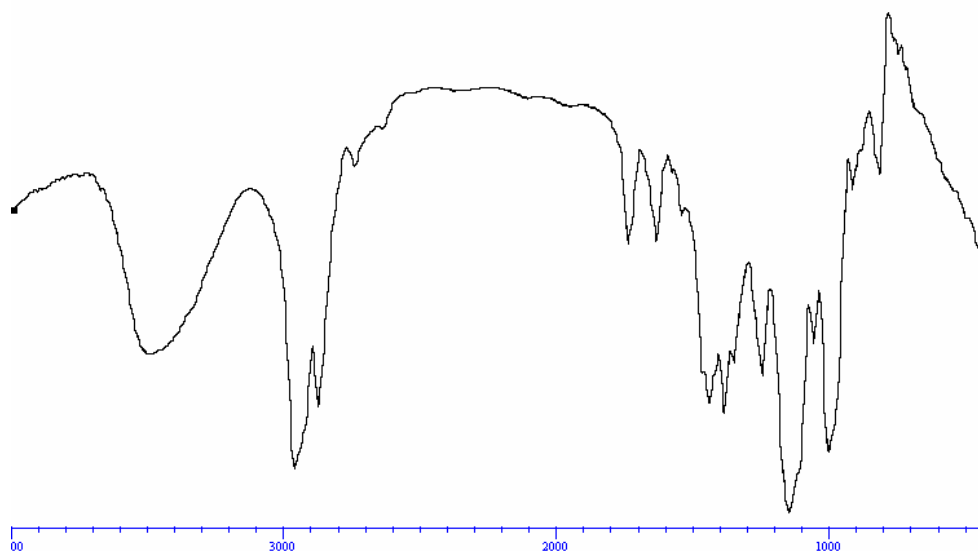


Figure 4.10 FT-IR spectra of Polyvinyl butyral ³⁶

From Figure 4.11. displaying the FT-IR spectrum of Polyethylene glycol, very dense resonance peaks around 1200 cm^{-1} are observed, proving the existence of polyethylene glycol in the tape cast polymer solution.

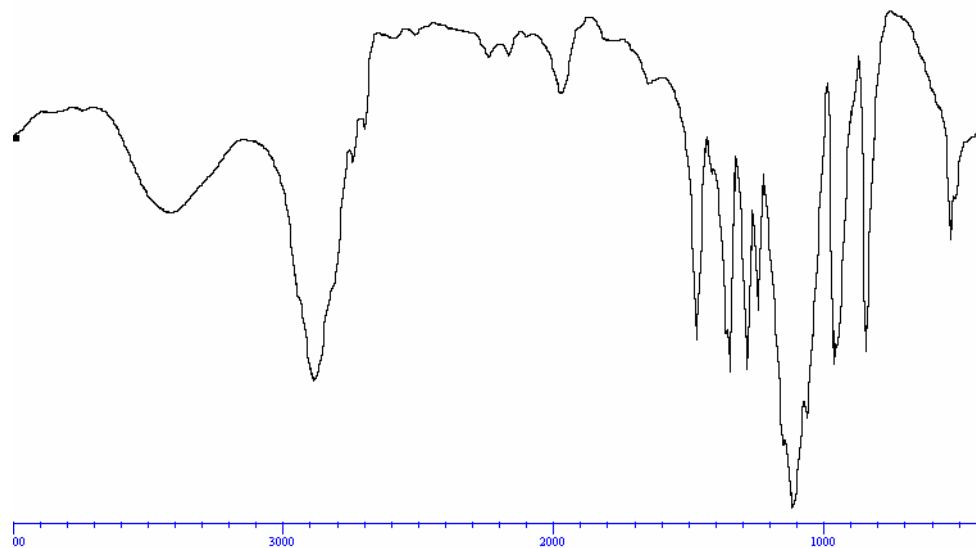


Figure 4.11 FT-IR spectrum of Polyethylene glycol Mw. 1500³⁷

Analyzing the DSC measurement results in Figure 4.12 and Figure 4.13, since there is more than one component in the tape cast polymer solution, existence of peaks in the DSC measurements was inconclusive.

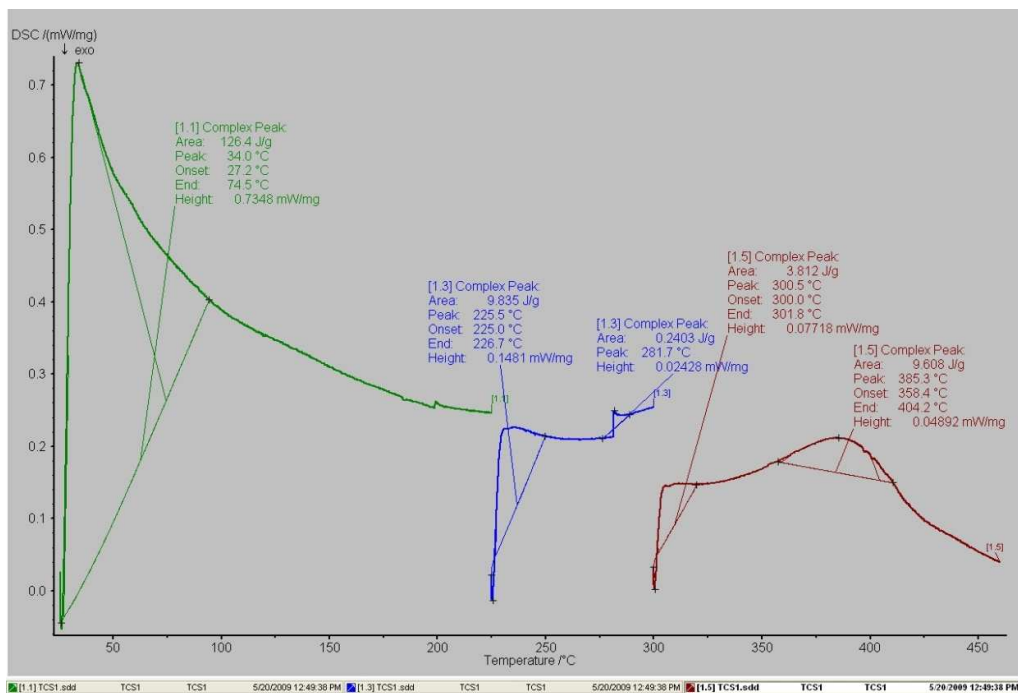


Figure 4.12 DSC thermogram of the tape cast polymer solution with isothermal steps

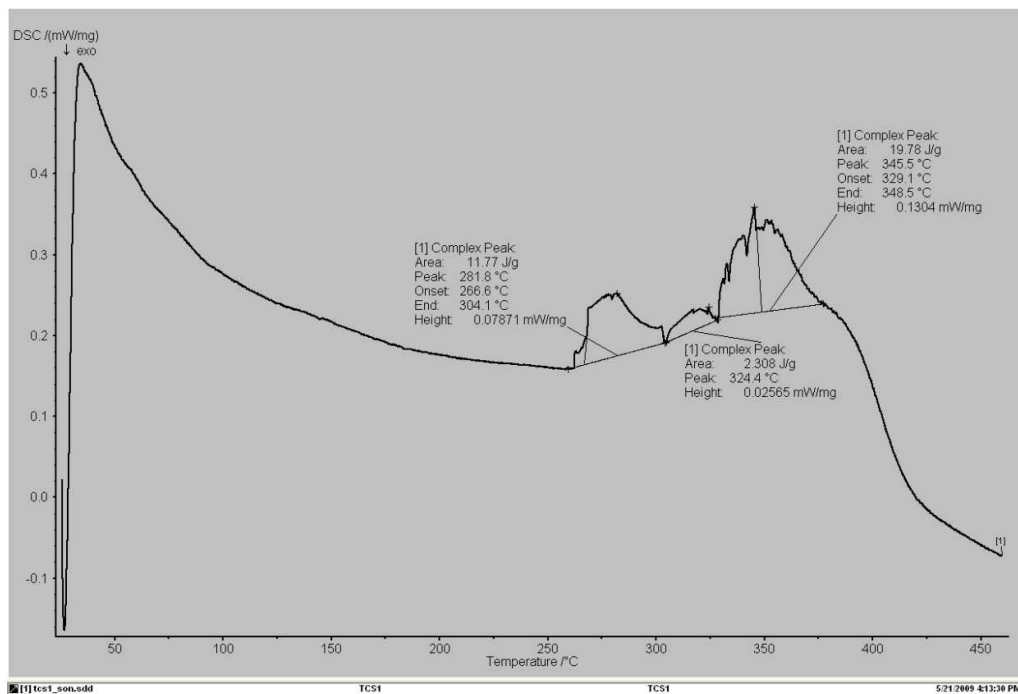


Figure 4.13 DSC thermogram of the tape cast polymer solution from room temperature up to 450°C.

In Figure 4.14, TGA measurement of the pure polymer solution is depicted. It is observed from the measurements that polymer begins to burn at the temperature of 270°C and loses around 90% of its mass at the temperature of 470°C.

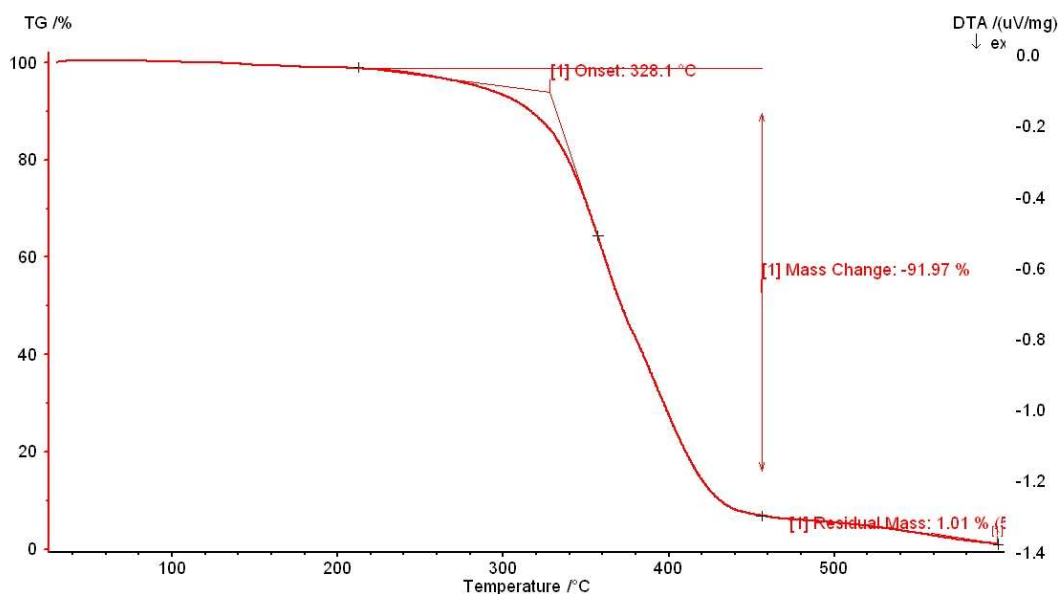


Figure 4.14 TGA measurement of the tape cast polymer solution from room temperature up to 450 °C.

From the EDS measurements shown in Figure 4.15, although precise information about the components could not be deferred, clear C and O peaks are observed prompting for the existence of polymer in the solution.

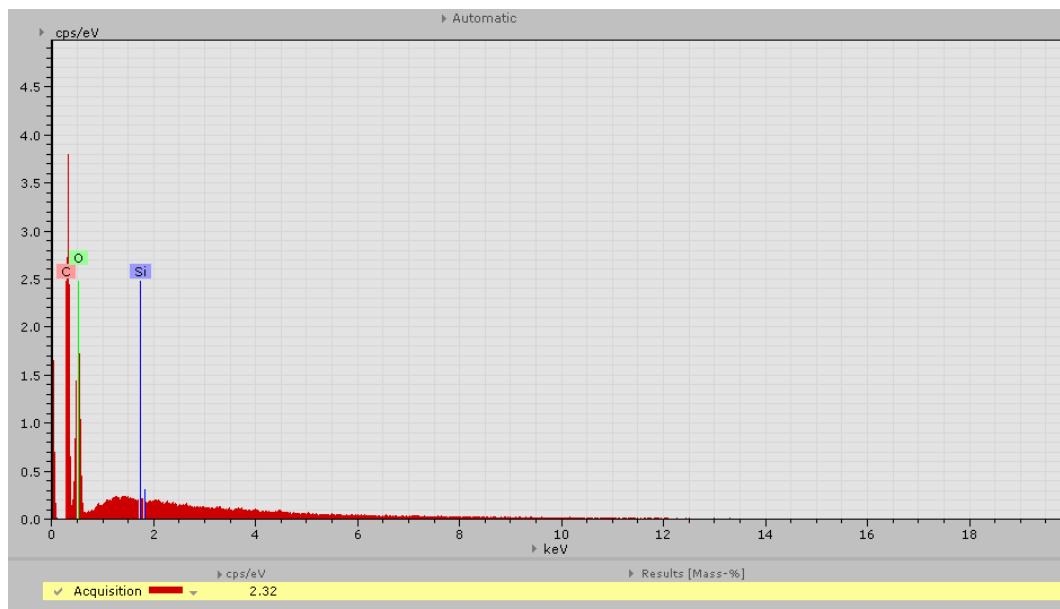


Figure 4.15 EDS measurement of the dry tape cast polymer solution

As for the dielectric measurements of the tape cast polymer solution, the same tape casting steps applied for the ceramic-polymer mixture films throughout the thesis were followed for the pure polymer solution itself. After stirring same amount of tape cast polymer solution in a magnetic stirrer in order to evaporate the excess solvent until the desired viscosity was obtained for the tape casting, slurry was cast with the same thickness as used earlier, i.e., on the order of 130 μm , for tape cast ceramic-polymer films. After obtaining tape cast films of the polymer, it was pressed with the same pressure in order to get rid of possible air bubbles trapped between the layer of films.

Dielectric constant measurements were carried out using the Agilent 16451B Impedance Analyzer. Results are shown in Figure 4.16 and Figure 4.17. It is observed that the dielectric constant of the polymer in the ceramic polymer composite tape cast film is approximately ~ 5.5 within the 15 MHz to 30 MHz frequency range with an average loss tangent of almost 0.12.

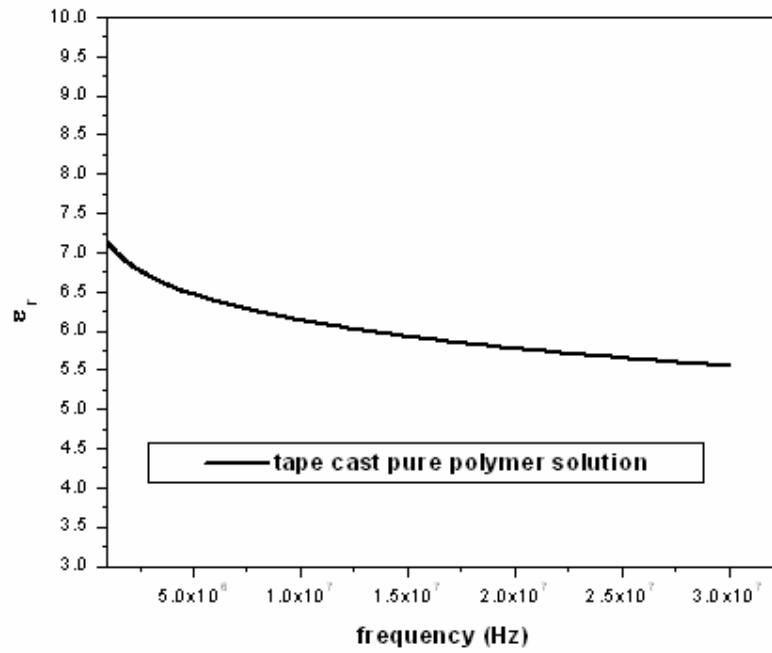


Figure 4.16 Dielectric constant vs. frequency (Hz) of tape cast polymer film made of pure polymer solution

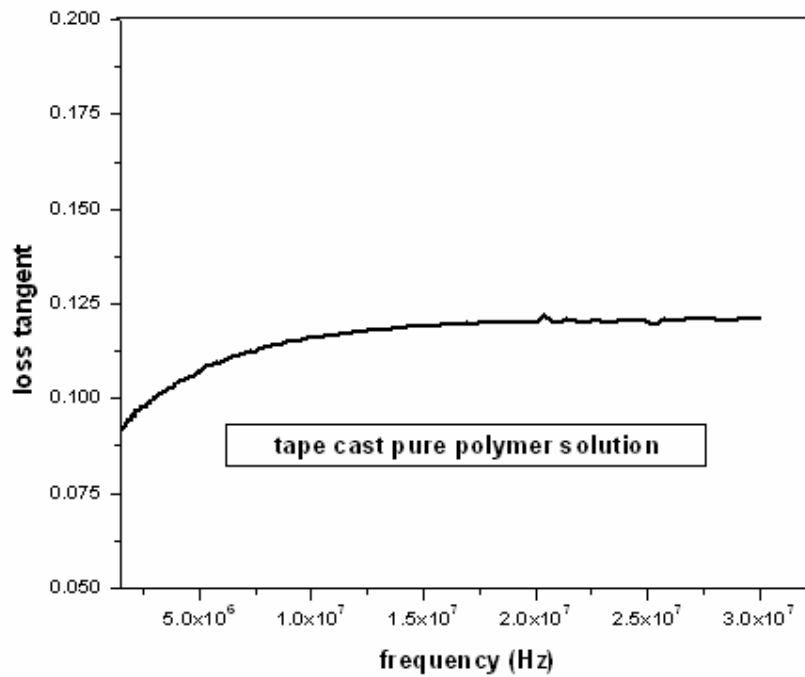


Figure 4.17 Loss tangent vs. frequency (Hz) of tape cast polymer film made of pure polymer solution

4.3. Analysis of Tape Cast Ceramic-Polymer Film Properties:

Knowing the dielectric constant and loss limitation of the constituent ceramic powder and the effect of pre-heat treatment on the powder pressed pellets, similar analyses were made for tape cast films produced using four different processes of the MCT 70 and MCT20 powders: 1) as-is powders, 2) pre-heat treated powders at 550°C (burn-out temperature) and 3) pre-sintered powders at 1360°C tape cast a) after ball-milling (uniform) or b) pounding in a mortar (non-uniform) to analyze the effect of partial or full sintering conditions on the ceramic constituent and hence the ceramic-polymer films.

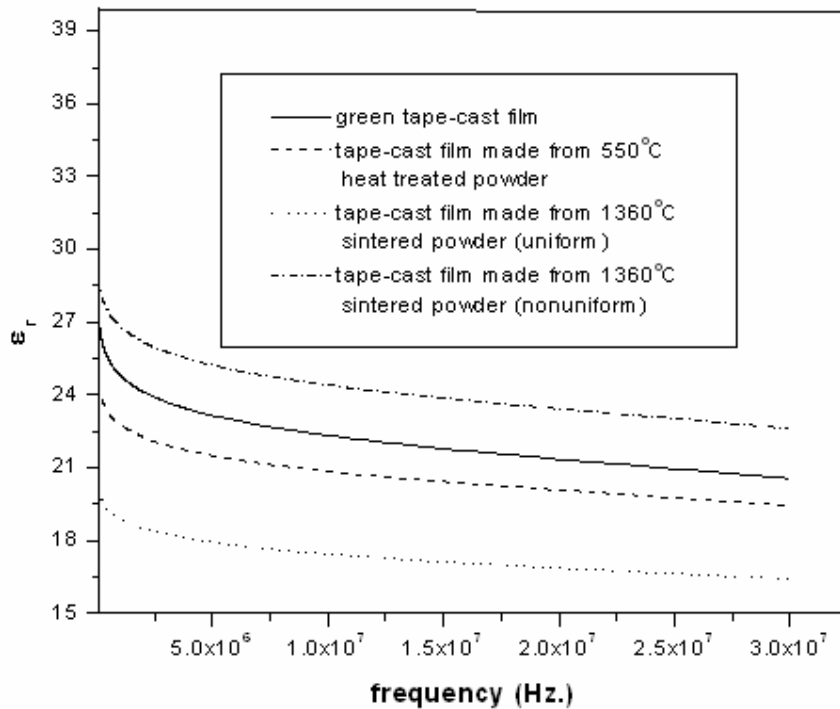


Figure 4.18 Dielectric constant vs. Frequency (Hz) of MCT70 ceramic powders produced via three different processes and made into tape cast films

Dielectric constant measurement is shown in Figure 4.18 for MCT70 material. As shown in Figure 4.18, dielectric constant value reaches ~ 24 for films made from spray dried ceramic powder and decreases to ~ 17 for films made from powder pre-sintered at 1360°C. Also, pre-heat treatment temperature and powder processing have a tuning effect on the resulting dielectric constant of the composite film with a non-uniform

powder processing combined with pre-heat treatment yielding an increase in dielectric constant.

As for the loss tangents measurements shown in Figure 4.10, it is observed that a film with a high dielectric constant in Figure 4.9 is accompanied with a high loss tangent value with the lowest loss tangent value observed for films made from 1360°C sintered powders which were ball-milled before tape cast. The only exception is observed for non-uniform powder films which are pre-sintered at high temperatures. Therefore, the effect of pre-heat treatment and powder processing before tape casting needs further investigation. What is meant by uniformity is that after sintering the MCT powders up to 1360°C, powders become so dense such that some grinding and ball milling took place to make it powder again before the tape casting process. As a result, after two times of ball milling, uniform tape cast films were obtained. As sintering of MCT's is observed to reduce the grain size and produce a more uniform microstructure, loss value decreases, but the same deduction is not valid for the dielectric constant value. Based on comparison of powder pellets and tape cast film behavior in Figure 4.4 and Figure 4.19, respectively, there is an overall increase of loss tangent value by a factor of 10.

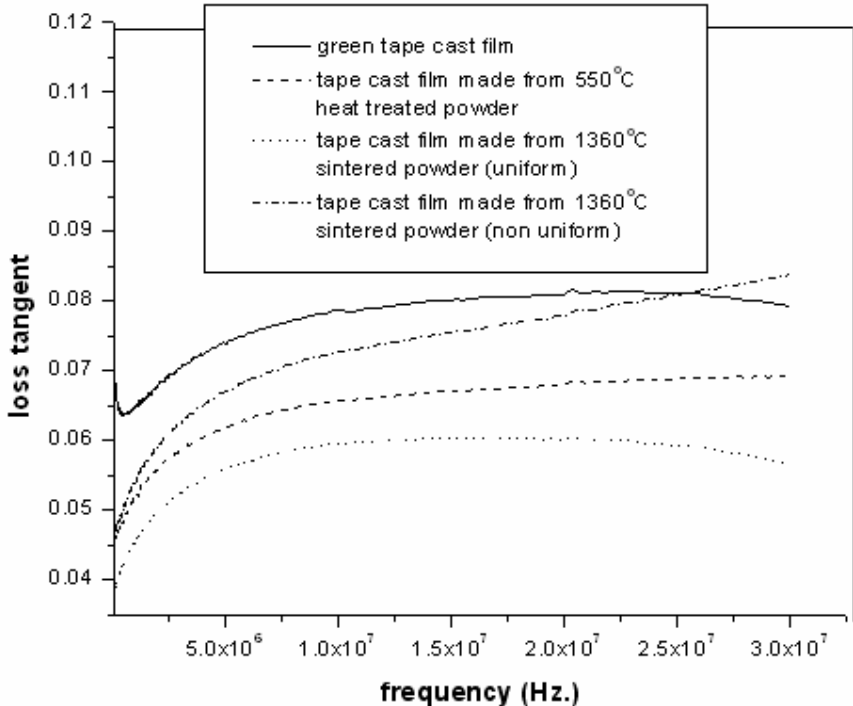


Figure 4.19 Loss tangent vs. frequency of MCT70 ceramic powder made tape cast films in four different process

As for the MCT20 ceramic powders, shown in Figure 4.20, dielectric constant value reaches ~10 for films made from spray dried ceramic powder and increases to ~12 for films made from powder pre-heat treated at 550°C (polymer burn-out temperature). Again, it is observed that pre-heat treatment temperature and powder processing have a tuning effect on the resulting dielectric constant of the composite film with a non-uniform powder processing combined with pre-heat treatment yielding an increase in dielectric constant value.

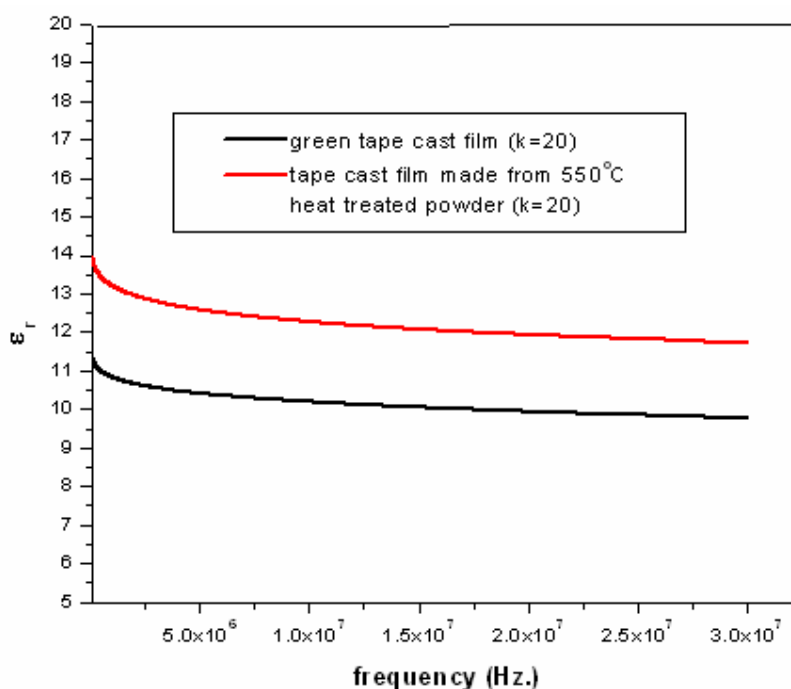


Figure 4.20 Dielectric constant vs. frequency (Hz) of MCT20 ceramic powders produced via two different processes and made into tape cast films

As for the loss tangent values shown in Figure 4.21, it is observed that a film with a high dielectric constant as shown in Figure 4.20 is accompanied with a high loss tangent value where the lowest loss tangent value was exhibited by films made from 550°C heat treated powders.

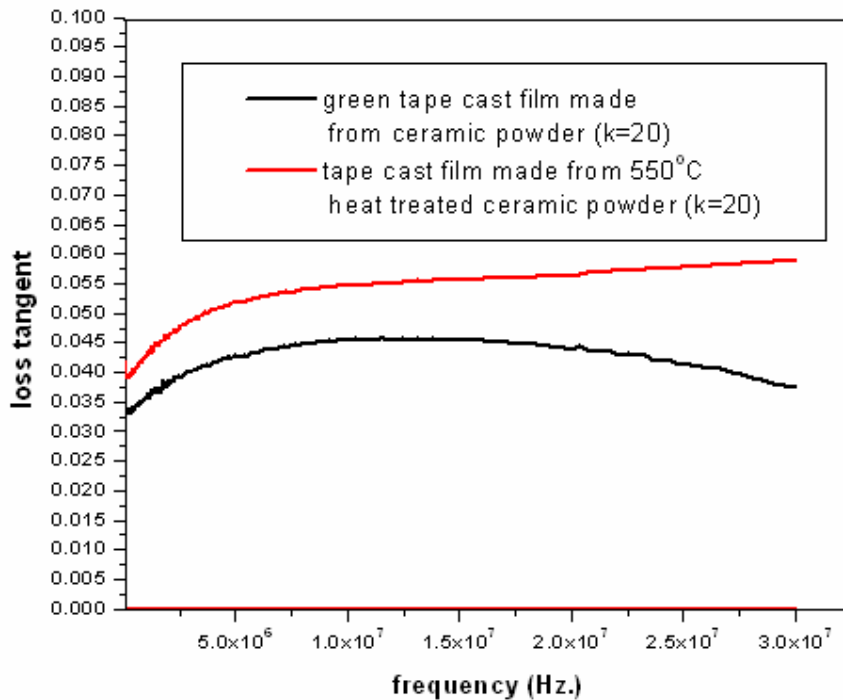


Figure 4.21 Loss tangent vs. frequency of MCT20 ceramic powder made tape cast films in two different processes

Before these tape cast films were used in making mosaic substrates, dielectric measurements were carried out for tape cast films made of spray dried $k=15$ and magnetic powder as shown in Figure 4.22. The permittivity of $k=15$ is observed to display the maximum permittivity of about 20 due to its carbon content. The carbon content corresponds to commercially available Sigradur K glossy Carbon microspheres, with an average particle size of 20 microns. As for magnetic flakes, permittivity of tape cast films were observed to be lower around $k=9$ with much lower loss tangent values for the magnetic tape cast films than for the $k=15$ films as depicted in Figure 4.23.

Since commercially MCT powders were not available with a dielectric constant less than 20 and carbon evaporates at low temperatures, the $k=15$ material was one of the base materials used earlier for producing a mixture with $k=15$ using carbon tat was to be evaporated and $k=20$. The resulting powder was then used for in Dry Powder Processing of sintered mosaic substrates. Similar to the other existing powders, the

approximate agglomerate size of the magnetic powders (Ni based ferrites) is around 20 to 100 microns.

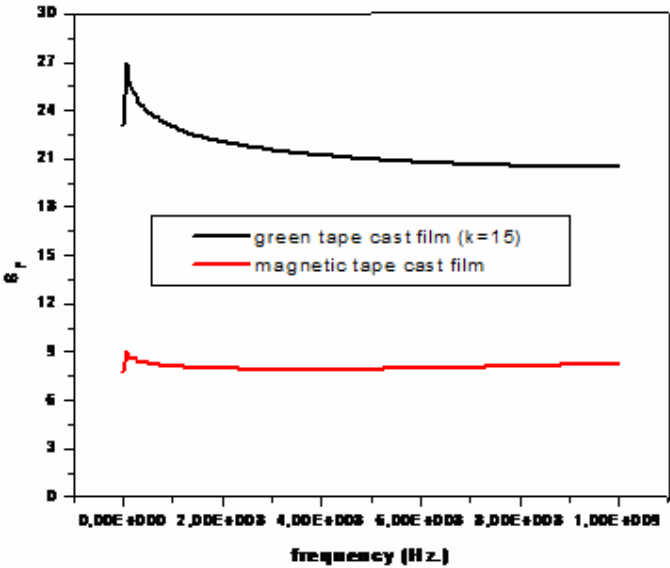


Figure 4.22 Dielectric constant vs. frequency (Hz.) of MCT15 and magnetic ceramic powders tape cast films

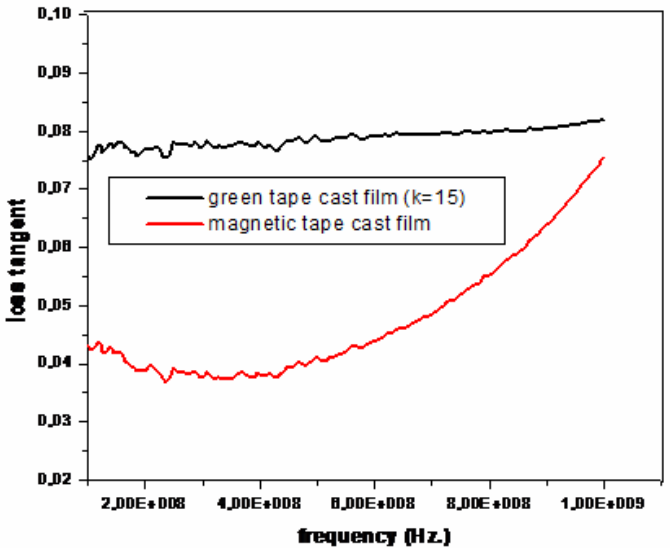


Figure 4.23 Loss tangent vs. frequency of MCT15 and magnetic ceramic powder tape cast film

4.4. Microstructural Analysis of Ceramic Powders and Tape Cast Films

Microstructures of two basic constituents namely spray dried MCT 20 and MCT 70 powders were analyzed via scanning electron microscopy and powder particles were observed to have a distribution as shown in Figure 4.24 with their particle size ranging from 20 to 100 μm .

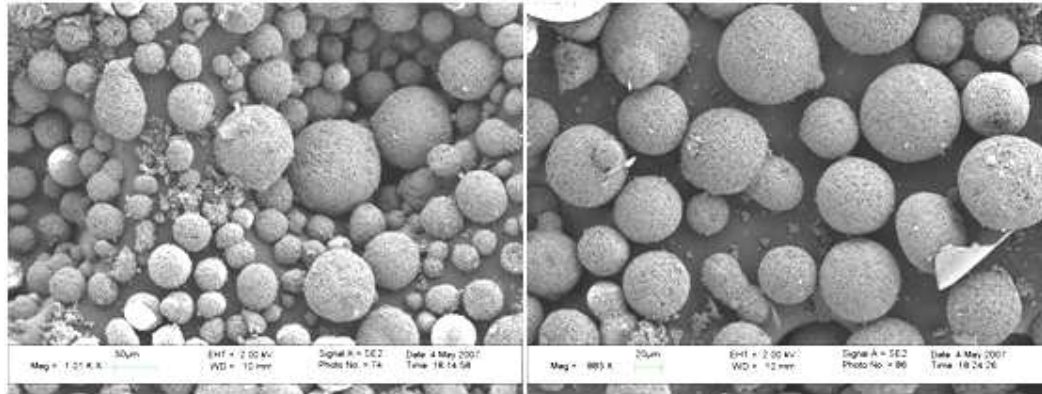


Figure 4.24 SEM image of MCT70 ceramic powder and MCT20 ceramic powder

Second, the microstructure of the ceramic powders, both MCT20 and MCT70, pellets were investigated. The microstructure images support their dielectric measurement behavior. As it can be seen from Figure 4.25, the highest dielectric constant sample has the densest microstructure with less air gaps between the particles. While the microstructure is becoming less dense, the dielectric constant decreases due to the air induced into the microstructure.

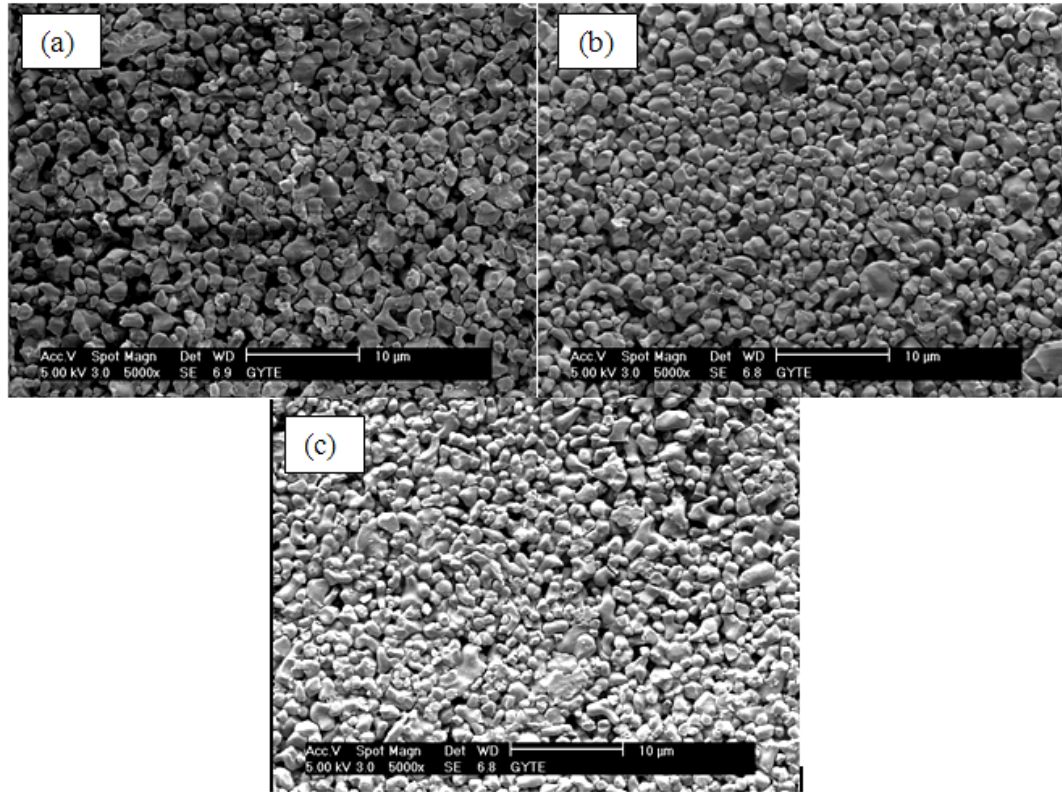


Figure 4.25 (a) SEM image of MCT20 ceramic powder as in pressed pellet from, (b) post-heat treated pellet at 550°C (polymer burn-out temperature) (c) pre-heat treated powder pellet at 550°C (polymer burn-out temperature) for 1 hr

As for the microstructure of the tape cast films made of MCT20, shown in Figure 4.26, SEM revealed good adhesion between the polymer (binder) and the ceramic particles for tape cast green films. Although some agglomerations were observed, in general it was noted that there was a uniform distribution of ceramic particles in the polymer matrix. When the same sample was heat treated to the polymer burn-out temperature of 550°C for 1 hr, polymer evaporated partially and ceramic agglomerates were observed.

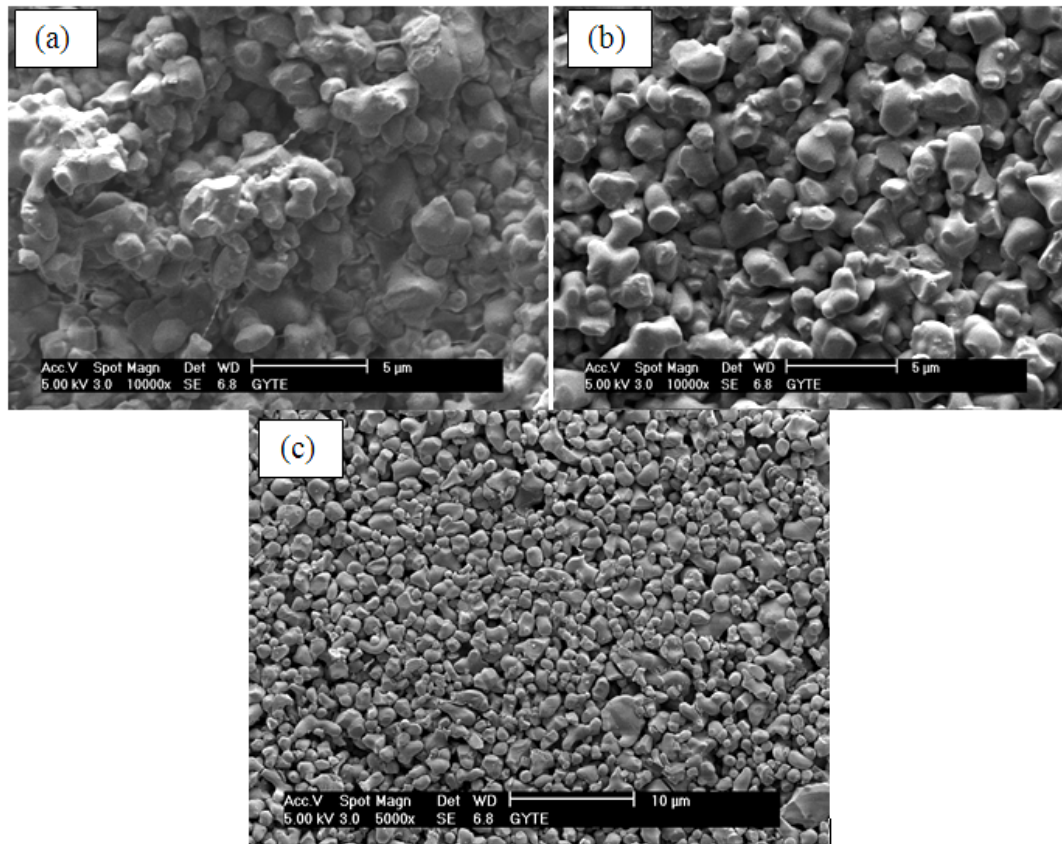


Figure 4.26 (a) MCT20 ceramic- polymer composite tape cast films as in the green state, (b) as made from the heat treated powder at 550°C (polymer burn-out temperature) for 1 hr, and (c) as post-heat treated tape cast film at 550°C polymer burn-out temperature) for 1 hr

In addition to the MCT20 ceramic polymer composite films, tape cast films made from MCT70 dielectric ceramics were also investigated. As it can be seen in Figure 4.27, for tape cast films as in its green state, ceramic particles dispersed in the polymer matrix uniformly. When the ceramic particles were heat treated up to the polymer burn-out temperature at 550°C before the tape cast process, since the ceramic particles are in spray dried form, at this temperature spray dried polymer also volatilized so that ceramic particles did not maintain their uniform spherical structure anymore as shown in Figure 4.27 (b). As the tape cast films were heat treated up to polymer burn-out temperature of 550°C, solvent volatilized leaving only the ceramic agglomeration behind as observed in Figure 4.27 (c).

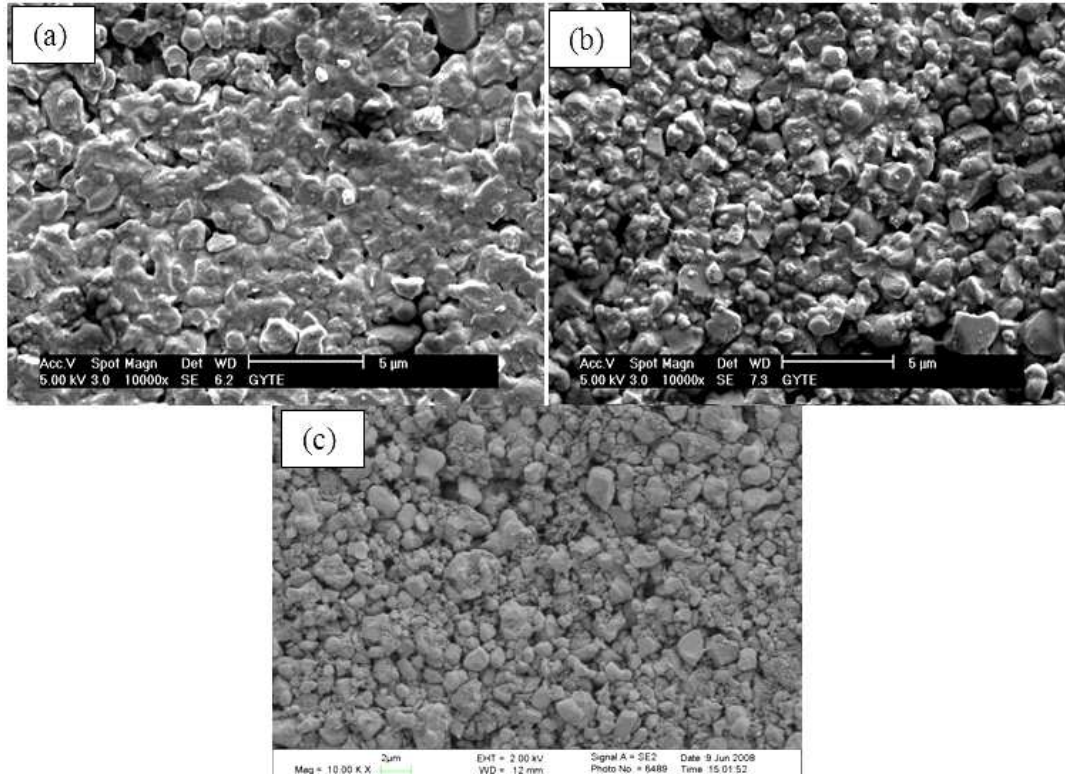


Figure 4.27 (a) SEM image of MCT70/polymer composite as it is in green state, (b) tape cast film made from pre-heat treated powder at 550°C polymer burn-out temperature) for 1 hr. and (c) post-heat treated tape cast film at 550°C polymer burn-out temperature) for 1hr

4.5. Antenna Performance Measurements

After the tape cast films made from different dielectric constant ceramic powders were produced, three different processes were used to create spatially variable substrates for antennas as explained in Section 3.5.

In this section measurement results for four different antennas made using the resulting spatially variable substrates are presented. For each antenna, copper tape is coated on the substrate to produce the radiating patch and the antenna is fed by a coaxial cable.

To test the performance of the fabricated antennas, their return loss performances were measured using an Agilent E8362B Network Analyzer yielding a resonance of 4.5 GHz and 5.7 GHz for the antenna fabricated by the dice and assembly method shown in Figure 4.28. Even for an antenna that is not optimized for performance (patch, feed location should be designed for desired application), the patch delivered sharp

resonances at 4.5 and 5.7 GHz as shown in Figure 4.29. Specifically resonances are observed at 4.3 GHz, 5.0 GHz, and 5.7 GHz.

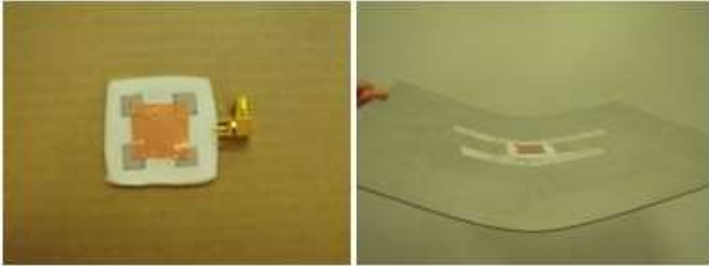


Figure 4.28 Antenna on substrate fabricated using the dice and assembly method

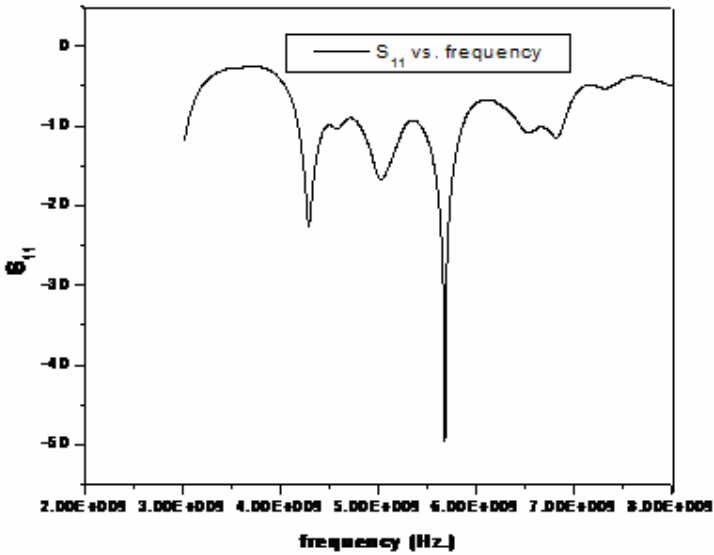


Figure 4.29 S₁₁ (dB) vs. frequency (Hz) for the antenna made of the substrate in Figure 4.28

Although the data around 2 GHz could not be recorded, the measurements for the resulting frequencies are in agreement with simulations with a shift about 300 MHz as

shown later in Figure 4.49 and Figure 4.50. This shift is most likely a result of the patch and substrate dimension inaccuracies during fabrication.

The second antenna which was measured was produced from the substrate fabricated by the dice and assembly method to yield a conformal substrate in 2D with three shades of tape cast films as shown in Figure 4.30.

The theoretical resonance frequency of the substrate can be estimated to compare it to the simulated and measured results using the following formulas based on the volumetric mixture rule for the effective dielectric constants of multi-material dielectric substrates:

$$\epsilon_{eff.} = \epsilon_a \frac{A_a}{A_{total}} + \epsilon_b \frac{A_b}{A_{total}} + \epsilon_c \frac{A_c}{A_{total}} \quad (7)$$

Where A_a , A_b , A_c represent the area of the material a, b, c (having dielectric constants of 21, 19 and 9 for the three shades of MCT70, MCT15 and MCT20, respectively) and A_{total} represents the total substrate area. It is noted that areas are used instead of volume ratios since the material inclusions in the substrate are of equal thickness.

$$\epsilon_{eff.} = 21 \frac{0.001065}{6.226 \times 10^{-3}} + 19 \frac{0.001961}{6.226 \times 10^{-3}} + 9 \frac{0.0032}{6.226 \times 10^{-3}} \quad (8)$$

$$\epsilon_{eff.} = 3.5921 + 5.9844 + 4.625 = 14.2 \quad (9)$$

From the definition of wavelength in guided media, the resonance frequency of the antenna can be calculated based on the effective dielectric constant ϵ_{eff} and wavelength corresponding to twice of the patch length of the antenna at resonance as the following:

$$\lambda = \frac{c}{f\sqrt{\epsilon_{eff}}} \quad (10)$$

Where c is the speed of light = 3×10^8 m/s.

Resonance wavelength λ can be approximated by two times the patch length as:

$$\lambda = 2 \times (0.025) = 0.050m \quad (11)$$

Hence,

$$f = \frac{3 \times 10^8}{0.050\sqrt{14.2}} = 1.59 \times 10^9 = 1.59GHz \quad (12)$$

From these results, it is concluded that theoretical results are in agreement with measurements shown in Figure 4.31.



Figure 4.30 Antenna on substrate in Figure 3.10 fabricated using the dice and assembly method

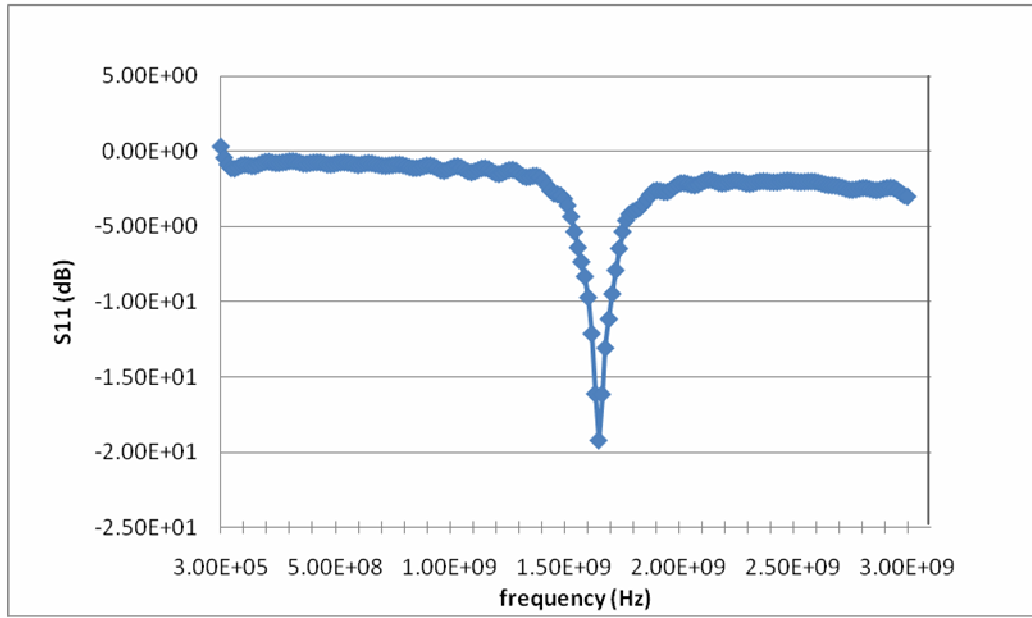


Figure 4.31 S_{11} (dB) vs. frequency (Hz) response for the antenna made of the substrate in Figure 4.30 as in the undeformed state

The same antenna was also measured in deformed state and it was observed that the matching changes about 10 dB, with the antenna still resonating at the same frequency of 1.60 GHz, as shown in Figure 4.32.

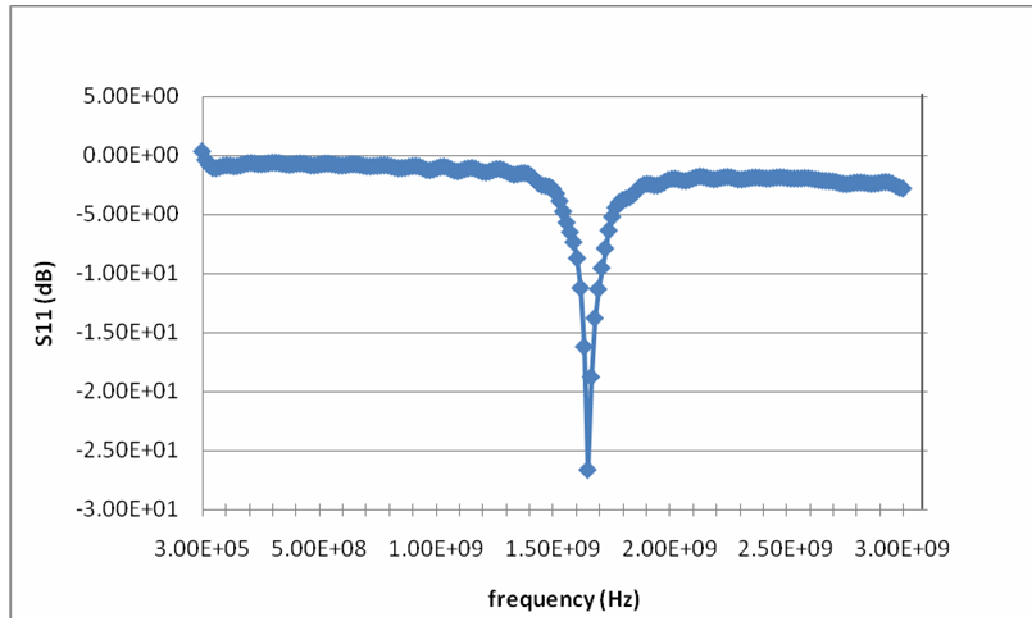


Figure 4.32 S_{11} (dB) vs. frequency (Hz) response for the antenna made of the substrate in Figure 4.19 as in the deformed state

The third antenna measurement was done for an antenna on the 2D spatially variable conformal substrate produced using the second fabrication method and is shown in Figure 4.33.



Figure 4.33 Antenna on substrate in Figure 3.11 fabricated using the second fabrication method

The measurement results of the antenna in undeformed and deformed states are shown in Figure 4.33 and Figure 4.35, respectively. It is observed that the antenna resonates at a frequency of 1.5 GHz, and has a S_{11} value of -20 dB.

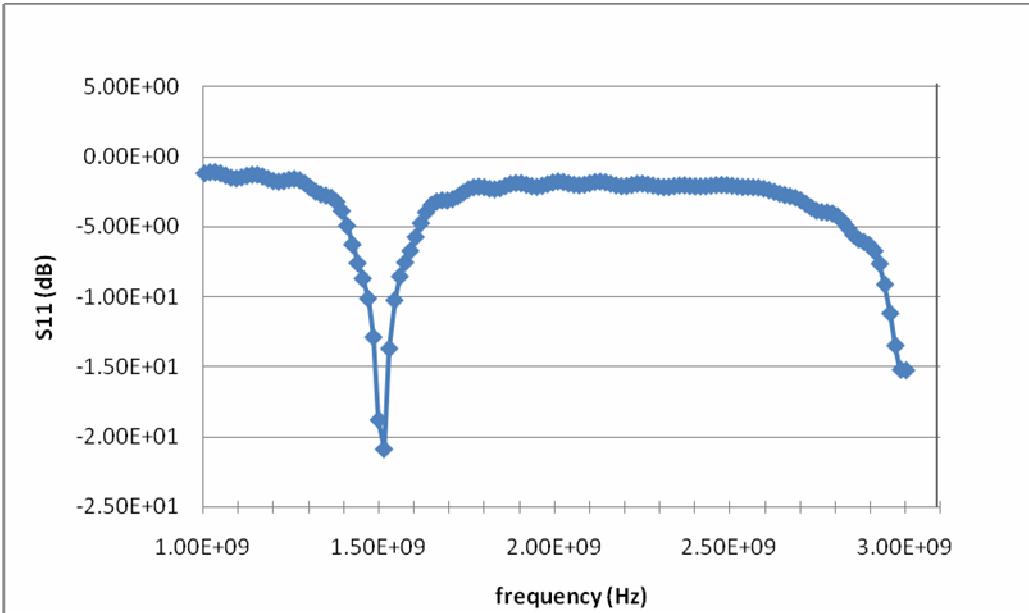


Figure 4.34 S_{11} (dB) vs. frequency (Hz) response of the antenna in Figure 4.33 as in the undeformed state

The same antenna but in the deformed state was measured and found that only the resonance matching does not change and the antenna still resonates at the same frequency of 1.50 GHz.

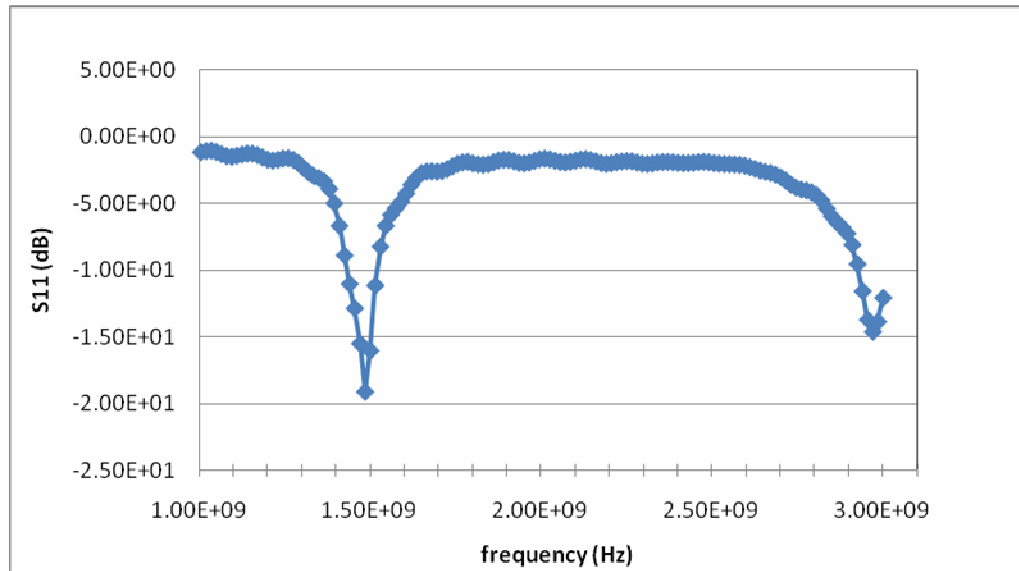


Figure 4.35 S11 (dB) vs. frequency (Hz) response of antenna in Figure 4.33 as in the deformed state.

Another measurement was carried out with the antenna on the substrate shown in Figure 4.37. Since the size of the patch and substrate is very small compared to other substrates, the resonance frequency was expected to be much higher than the previous substrates, so another network analyzer, namely Agilent 8720ES was used and is shown in Figure 4.36.



Figure 4.36 Agilent 8720ES Network Analyzer

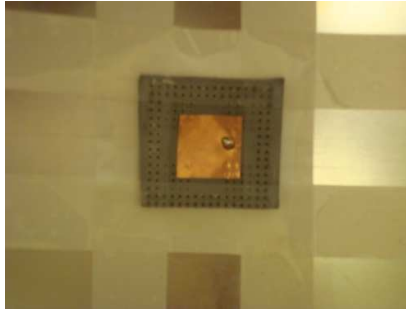


Figure 4.37 Antenna on substrate in Figure 3.14 fabricated using the drill and fill method

The same antenna was also measured in the deformed positions with horizontal and vertical bending positions (according to feed location) in order to understand the effect of bending direction on the antenna performance outputs such as matching and resonance frequency values and respective results are shown in Figure 4.39 and Figure 4.40.

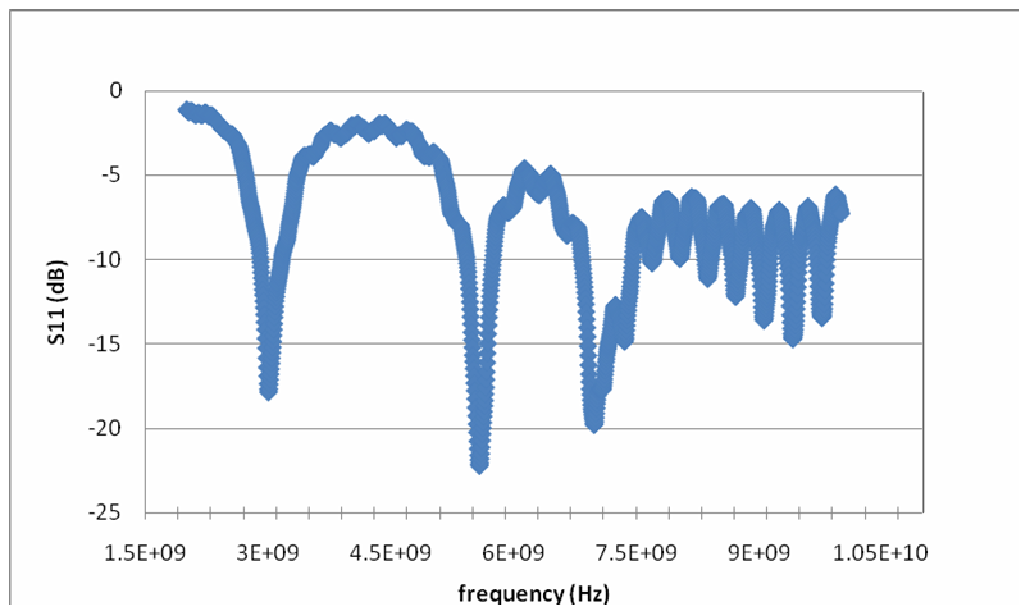


Figure 4.38 S_{11} (dB) vs. frequency (Hz) response of the antenna in Figure 4.37 as in the undeformed (flat) state

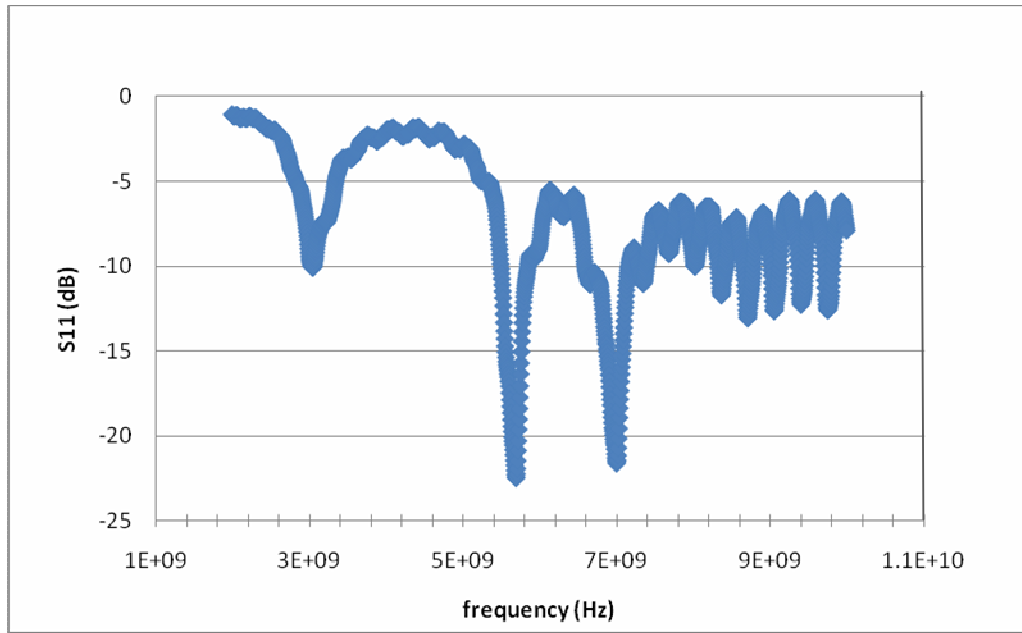


Figure 4.39 S_{11} (dB) vs. frequency (Hz) response of the antenna in Figure 4.37 as in the horizontal bended position according to feed location in the patch

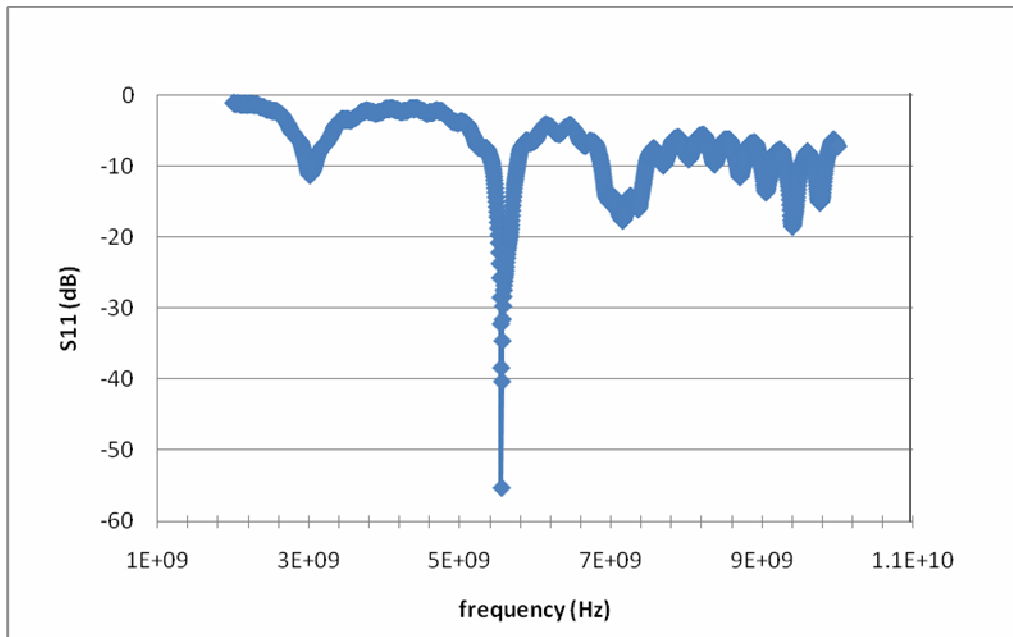


Figure 4.40 S_{11} (dB) vs. frequency (Hz) response of the antenna in Figure 4.37 as in the vertical bended position according to feed location in the patch

As can be seen from Figures 4.38, 4.39 and 4.40, deformation of the antenna did not have an effect on the resonance frequency but on the resonance matching. Vertical bending of the patch antenna according to the feed location on the patch improved the matching ability where in all cases the resonance frequency stayed the same. Resonance frequencies were observed at the following values: 3.24 GHz, 5.73 GHz and 7.52 GHz.

Finally, an antenna on the substrate which was fabricated by the drill and fill process was measured and is shown in Figure 4.41 yielding a first resonance around 3.32 GHz.

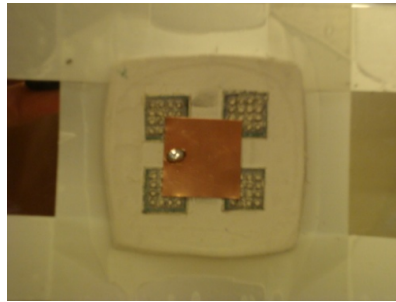


Figure 4.41 Antenna on substrate in Figure 3.13 (b) fabricated using the drill and fill method

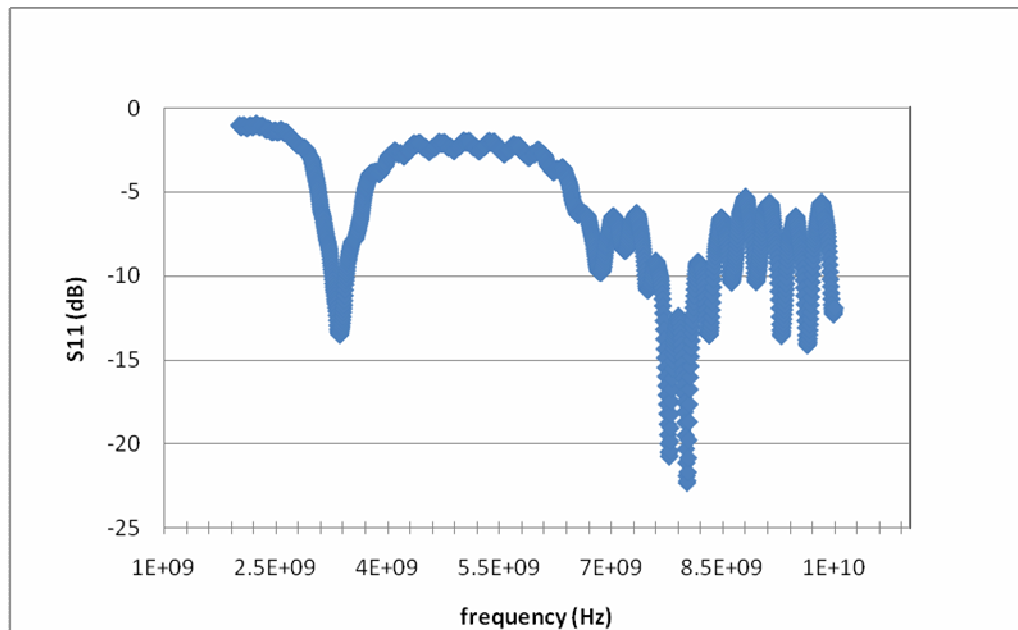


Figure 4.42 S11 (dB) vs. frequency (Hz) response of the antenna in Figure 4.41 as in the undeformed state

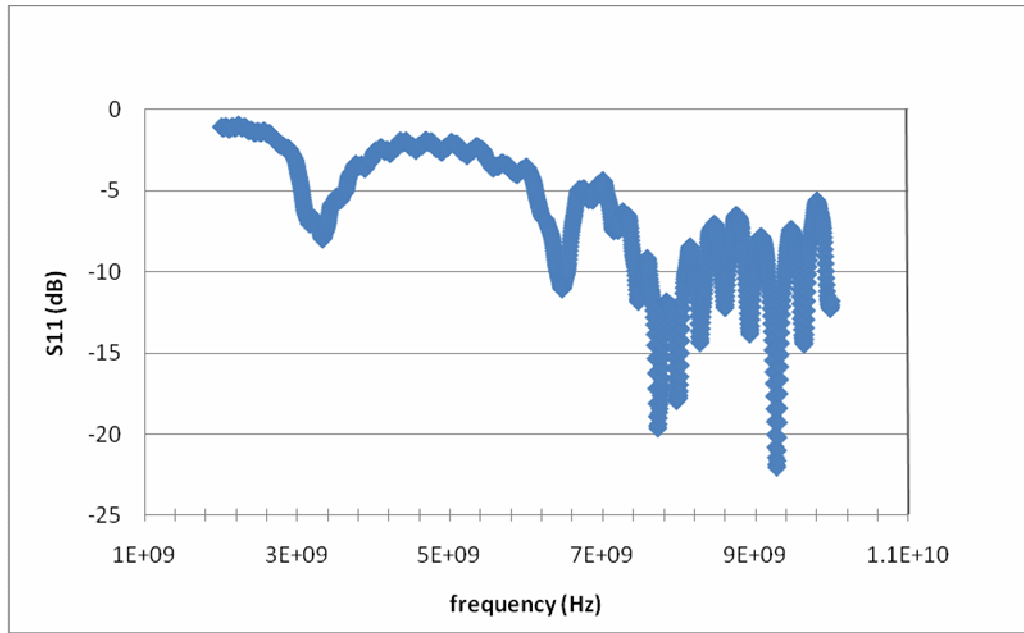


Figure 4.43 S_{11} (dB) vs. frequency (Hz) response of the antenna in Figure 4.41 as in the horizontal bended position

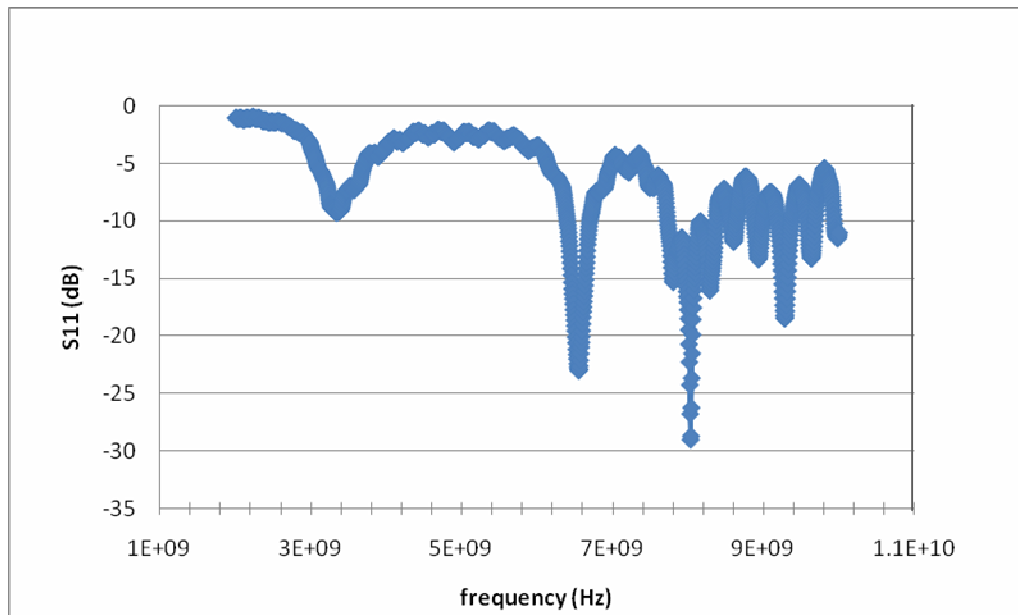


Figure 4.44 S_{11} (dB) vs. frequency (Hz) response of the antenna in Figure 4.41 as in the vertical bended position

To compare the performance of the antennas made on flexible spatially variable substrates of relatively high dielectric constants (higher than 10) discussed above with a patch antenna performance mounted on a standard uniform substrate of FR4 shown in Figure 4.45, similar return loss measurements were carried out for the latter. It is noted that the antennas on spatially variable substrates were smaller in size, specifically $1/5^{\text{th}}$ of an antenna printed on a standard FR4 substrate. This antenna exhibits a major resonance at around 1.5 GHz shown in Figure 4.46 similar to resonances of produced flexible mosaic substrates (such as shown in Figure 4.31 and Figure 4.32) proving the miniaturization capability of produced flexible substrates.



Figure 4.45 Antenna on fabricated spatially variable substrate (size=40 mm) left and on standard FR4 substrate (right) (size=200 mm)

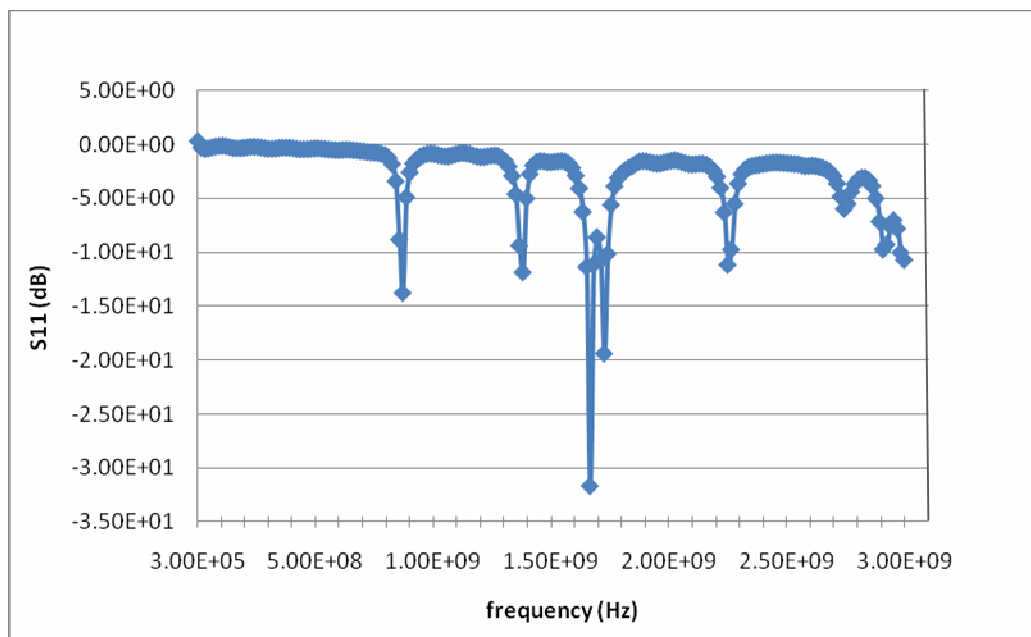


Figure 4.46 S_{11} (dB) vs. frequency (Hz) response of an antenna on a standard substrate FR4, shown in Figure 4.45 right

4.6. Antenna Performance Simulations

Antenna simulations were carried out for antennas shown in Figure 4.28 and Figure 4.30 using COMSOL Multiphysics version 3.5a. To simulate the performance of these antennas, a simple patch model was created on these substrates according to real physical dimensions and composition and their return loss response was simulated. Parametric solver type was used throughout the simulations, where the parameter was selected as the frequency. As the linear solver, direct solver type, specifically UMFPACK type solver was selected. For the antenna in Figure 4.28, mesh statistics were as tabulated in Table 4.1.

Table 4-1 Mesh Statistics for the antenna simulation on the substrate shown in Figure 4.28

Number of degrees of freedom		334696
Number of mesh points		9791
Number of elements		49678
	Tetrahedral	48430
	Prism	1248
	Hexahedral	0
Number of boundary elements		8133
	Triangular	7909
	Quadrilateral	224
Number of edge elements		1123
Number of vertex elements		156
Minimum element quality		0.0388
Element volume ratio		2.97E-07

For the antenna printed on the substrate as shown in Figure 4.28, the CAD model, 3D mesh and resulting field distribution is shown in Figure 4.47. Its transmitted power ratio (ratio of the radiated power to the input power) and return loss performances are shown in Figure 4.48 and Figure 4.49, respectively. The response indicated a resonance of ~2.2. GHz as expected for an effective epsilon of 9.9 proving the simulation's reliability.

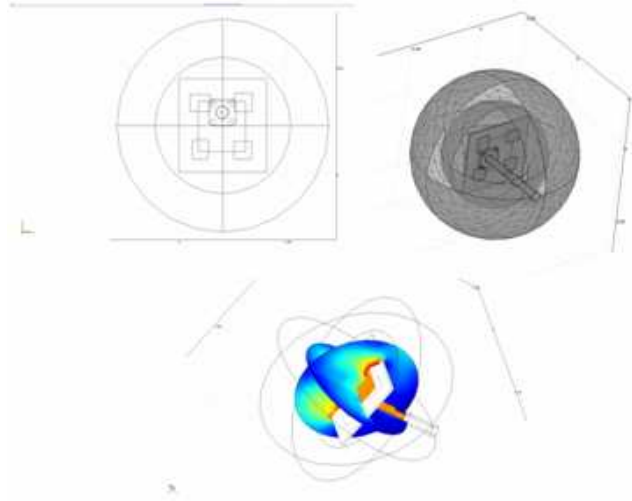


Figure 4.47 CAD Model, 3D Mesh of CAD, resulting field distribution for antenna in Figure 4.28

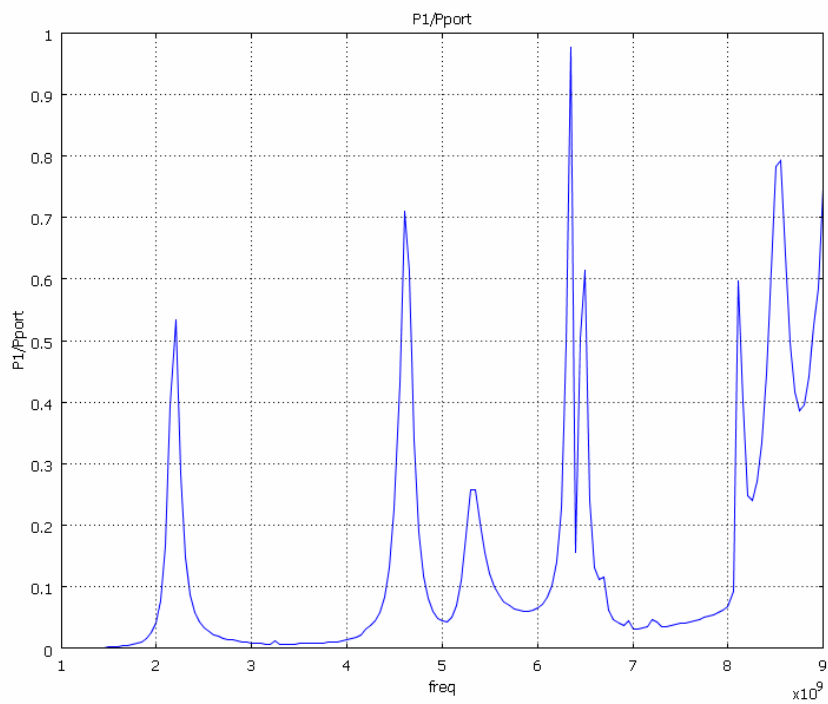


Figure 4.48 P1/Pport distribution simulations of antenna on substrate shown in Figure 4.28

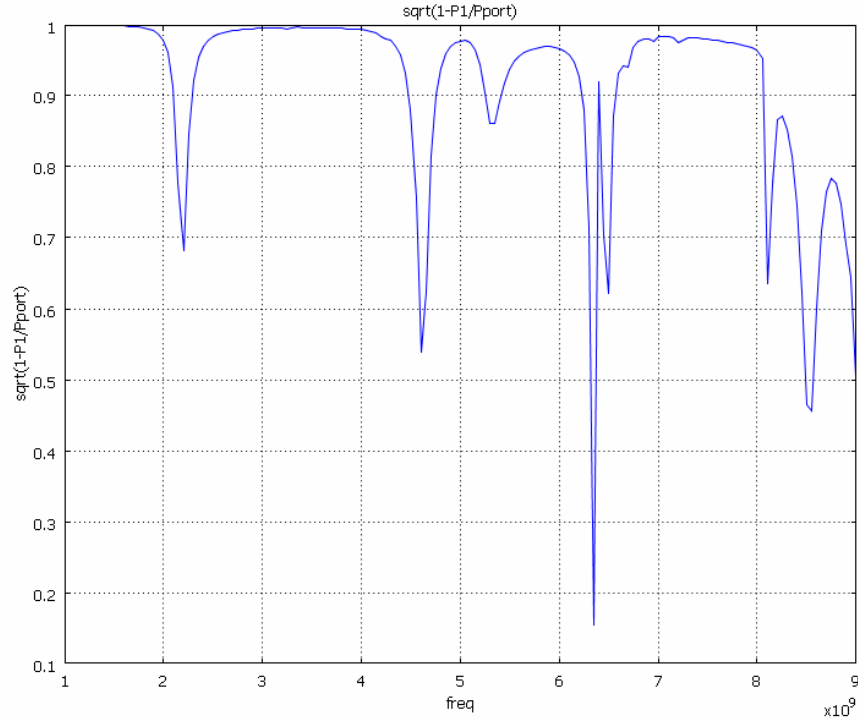


Figure 4.49 Return loss S_{11} (dB) vs. frequency (Hz) simulations of antenna printed on substrate shown in Figure 4.28

Although the data around 2 GHz could not be recorded during measurements and hence a one to one comparison for the first resonance was not possible with simulations, the resulting higher order mode frequencies of 4.6 GHz and 5.2 GHz for simulations and 4.3 GHz and 5.0 GHz for measurements close to simulations with a shift about 300 MHz. This shift is most likely the result of the patch and substrate dimension inaccuracies during fabrication and the inexact drawing capabilities in a simulation environment.

For the antenna in Figure 4.30, mesh statistics are given in Table 4.2. Simulation was carried out using COMSOL version 3.5a. Parametric solver type was used throughout the simulations, where the parameter was selected as the frequency. As the linear solver, direct solver type, specifically UMFPACK type solver was selected. Solution took approximately 12 hours using a Dell workstation with 64 GB memory and a 3.20 GHz CPU processor.

For the antenna printed on the substrate as shown in Figure 4.30, the CAD model, 3D mesh and resulting field distribution is shown in Figure 4.50. Its transmitted power ratio

(ratio of the radiated power to the input power) and return loss performances are shown in Figure 4.51 and Figure 4.52, respectively.

Table 4-2 Mesh Statistics for the antenna simulation on the substrate shown in Figure 4.30

Number of degrees of freedom	714606	
Number of mesh points	20443	
Number of elements	106806	
	Tetrahedral	103846
	Prism	2960
	Hexahedral	0
Number of boundary elements	17003	
	Triangular	16587
	Quadrilateral	416
Number of edge elements	2276	
Number of vertex elements	308	
Minimum element quality	2.72E-04	
Element volume ratio	5.68E-11	

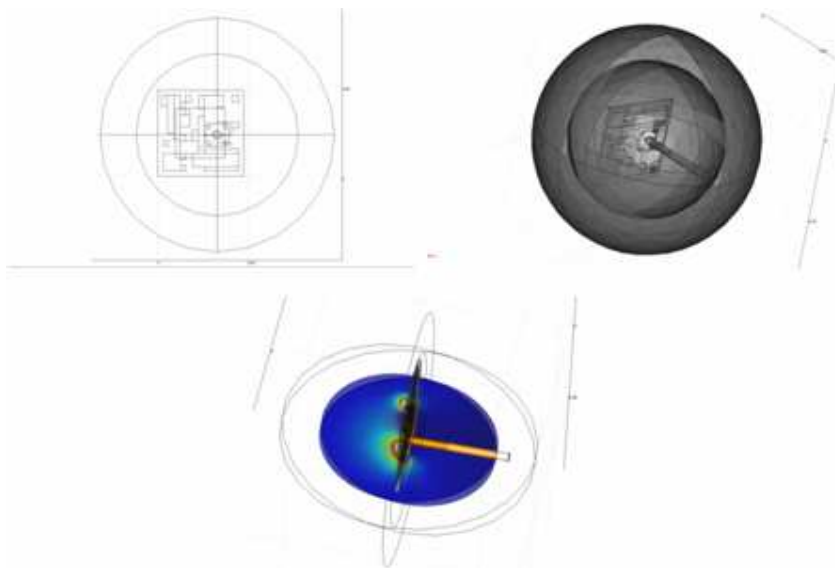


Figure 4.50 CAD Model, 3D Mesh of CAD, resulting field distribution for antenna in Figure 4.30

The response predicted a resonance of ~ 1.35 GHz as expected for an effective epsilon of 9.9 but with an underprediction by 250 MHz when compared with measurements in Figure 4.31.

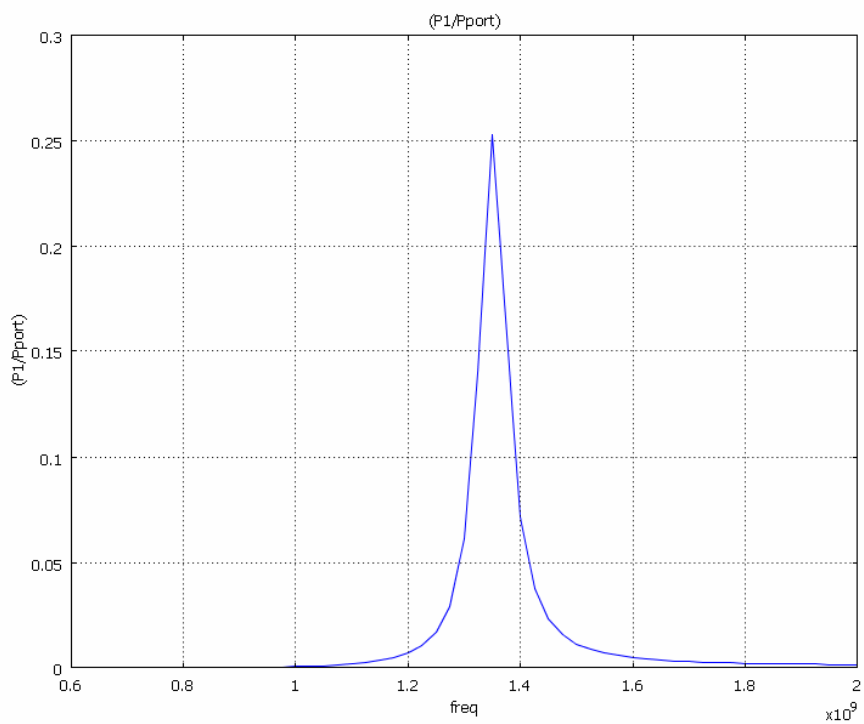


Figure 4.51 P1/PPort distribution of the antenna on substrate in Figure 4.30

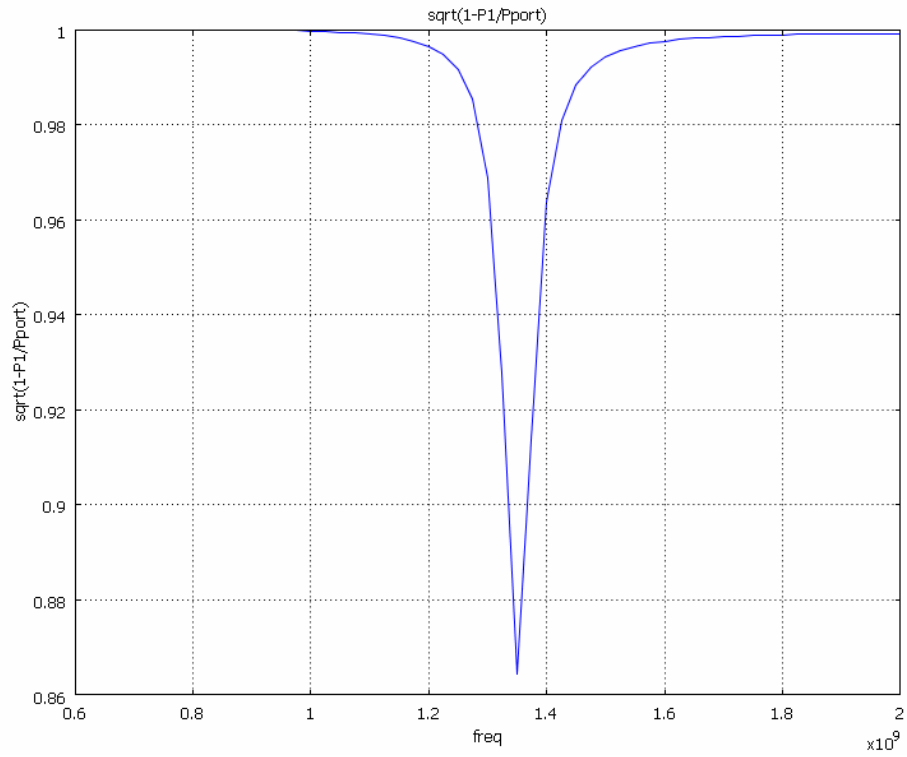


Figure 4.52 Return loss S11 (dB) vs. frequency (Hz) simulation result for antenna printed on substrate in Figure 4.30

CHAPTER 5

5. CONCLUSIONS & FUTURE WORK

In this thesis, flexible ceramic polymer composite substrates were fabricated using tape casting process, with the objective of producing relatively high dielectric constant and low-loss substrates to achieve miniaturization and flexibility for Radio Frequency applications. These substrate materials are characterized mainly based on measurements of dielectric constant, loss tangent and microstructure investigation using scanning electron microscope.

To achieve tunability, a heat treatment scheme of constituent powders prior to tape casting was investigated to analyze the effect on dielectric constant and loss. More specifically, various tape cast films were obtained through the process using ceramic powders sintered up to the full sintering temperature of 1360°C. These composite films were also heat treated to the burn-out temperature (550°C) to get rid of the binder to achieve high dielectric constant. Further sintering is not followed to attain a considerable amount of flexibility. Results show that the dielectric constant of MCT-70 polymer films can be tuned in the range of 12 to 23 with no sacrifice in dielectric loss. Similarly, MCT20 polymer films can be tuned in the range of 10.5 to 12 with dielectric loss tangent value of 0.040-0.055 and MCT15 polymer films can be tuned in the range of 19 to 21 with dielectric loss tangent value of 0.070.

Spatially variable conformal mosaic structure using tape cast film base materials are obtained using three methods: 1) Dice and Assembly method 2) Machining pores at desired locations per the spatial variation in tape cast green films and stacking them onto each other and 3) Drill and fill process.

Eventually, the fabricated substrates have been used to construct patch antennas and their resonance behavior was measured using Agilent network analyzers. In order to validate the measurements, antenna simulations were carried out and compared to

theoretical predictions. Antenna simulations were carried out using COMSOL Multiphysics 3.5a. Despite an 200 MHz to 300 MHz shift between measurements and simulations, results are very promising and prove the miniaturization and tuning capability of fabricated conformal substrates. Agreements of the measured effective permittivity and calculated results proves earlier measurement results of tape cast films and motivates further design studies where the substrate could be actually designed not only for miniaturization but also bandwidth and efficiency improvements.

Future work consists of the fabrication of mosaic substrates according to a specific design model, obtaining a complete 3D material variation using three methods stated above and fabrication of magnetic tape cast films. Remaining challenges constitute reducing loss factor by methods such as controlling particle size of ceramic powder. If successful, it has the potential to open up new paths in the production of miniaturized heterogeneous RF structures made of ceramic polymers composites integrated possibly with conductors as entire monolithic structures.

6. BIBLIOGRAPHY

- [1] M.A. Matin, B.S. Sharif, C.C. Tsimenidis (2007), "Microstrip patch antenna with matching slots for UWB communications", *Int. J. Electron. Commun.*: 6, 132 – 134.
- [2] K. Sarabandi, R. Azadegan, H. Mosallaei and J. Harvey, "Antenna Miniaturization Techniques for Applications in Compact Wireless Transceivers", Radiation Laboratory Department of Electrical Engineering and Computer Science, The University of Michigan, Ann Arbor, MI 48109-2122.
- [3] C. Marrmt, A. Moulart, J. Colton (2003), "Flexible Polymer Composite Electromagnetic Crystals", *Polymer Engineering and Science* : 23(4) 822-830.
- [4] F. Xiang, H. Wang , X. Yao (2007), "Dielectric properties of SrTiO₃/POE flexible composites for microwave applications", *Journal of the European Ceramic Society*: 27, 3093–3097.
- [5] S. Solomona, H. Padma Kumara, L. Jacob, J.K. Thomasc, M. R. Varma, (2007), "Ln(Zr_{1/3}Ti_{2/3})TaO₆ (Ln = Ce, Pr, Nd and Eu): A novel group of microwave ceramics" , *Journal of Alloys and Compounds*, doi:10.1016/j.jallcom.2007.07.083.
- [6] Y. Rao, J. Yue, C.P. Wong (2001), "Material characterization of high dielectric constant polymer-ceramic composite for embedded capacitor to RF application." *International Symposium on Advanced Packaging Materials: Processes, Properties and Interfaces, Proceedings*: 25, 123-129.
- [7] Z. Dong, C. Xiong, H. Quanb and G. Zhao (2006), "Polyvinyl-butyril/lead zirconate titanates composites with high dielectric constant and low dielectric loss", *Scripta Materialia* : 55, 835–837.
- [8] C.C. Wu, Y. C. Chen, C.F. Yang, C.C. Su, C.C. Diao (2007), "The dielectric properties of epoxy/AlN composites." *Journal of the European Ceramic Society*: 27, 3839-3842.
- [9] S. Koulouridis, G. Kiziltas, Y. Zhou, D. Hansford, and J. L. Volakis (2006), "Polymer-Ceramic Composites for Microwave Applications: Fabrication and Performance Assessment" *IEEE Transactions on Microwave Theory and Techniques*: 54 (12) 4202-4208.

- [10] J. Zhai, C. Gao, X. Yao, Z. Xu, H. Chen (2008), "Enhanced dielectric tunability properties of Ba(ZrxTi1-x)O-3 thin films using seed layers on Pt/Ti/SiO2/Si substrates." *Ceramics International*: 34(4) 905-910.
- [11] F. Xiang, H. Wang, M. Zhang, X. Sun, X. Yao (2008), "Preparation and dielectric tunability of bismuth-based pyrochlore dielectric thick films on alumina substrates." *Ceramics International*: 34(4) 925-928.
- [12] D.J. Hansford and K. H. Sandhage (2007), "Novel polymer-ceramic composites for conformable RF applications." *IEEE Antennas and Propagation Society International Symposium*: 1(12) 1574-1577.
- [13] S. Schwarzer, and A. Roosen (1999), "Tape casting of piezo ceramic polymer composites." *Journal of the European Ceramic Society*: 19(6-7) 1007-1010.
- [14] L. Wang, G. Tang, Z. K. Xu (2008), "Preparation and electrical properties of multilayer ZnO varistors with water-based tape casting", *Ceramics International*, doi:10.1016/j.ceramint.2008.01.011.
- [15] C. Ozturk, Y. K. Turk (2006), "Processing and mechanical properties of textured mullite/zirconia composites", *Journal of the European Ceramic Society* : 27 1463–1467.
- [16] P. S. Nealakanta (1995), "Handbook of Electromagnetic Materials, Monolithic and Composite Versions and their Applications", CNC Press.
- [17] W. D. Callister (2006), "Materials Science and Engineering An Introduction", Wiley.
- [18] P. M. Mendes, A. Polyakov, M. Bartek, J.N. Burghartz, J.H. Correia (2006), "Integrated chip-size antennas for wireless microsystems: Fabrication and design considerations." *Sensors and Actuators a-Physical*: 125(2) 217-222.
- [19] I.S.Ghosh, I. S., A. Hilgers, T. Schlenker, R. Porath (2001), "Ceramic microwave antennas for mobile applications." *Journal of the European Ceramic Society*: 21(15) 2621-2628.

- [20] M.A. Matin, B. S. Sharif, C.C. Tsimenidis (2007), "Microstrip patch antenna with matching slots for UWB communications." *AEU-International Journal of Electronics and Communications*: 61(2) 132-134.
- [21] L. Boccia, G. Amendola, et al. (2007), "Performance evaluation of shorted annular patch antennas for high-precision GPS systems." *Iet Microwaves Antennas & Propagation* 1(2): 465-471.
- [22] C.S. Chen, C.C. Chou, W.J. Shih, K.S. Liu, C.S. Chen, and L.N. Lin (2003), "Microwave dielectric properties of glass- ceramic composites for low temperature cofirable ceramics", *Mater. Chem. Physics*: 79 129–134.
- [23] C.S. Chen, C.C. Chou, C.S. Chen, and I.-N. Lin. (2004), "Microwave dielectric properties of glass-MCT low temperature cofireable ceramics", *J. Eur. Ceram. Soc.* 24: 1795–1798.
- [24] Q.L. Zhang, H. Yang, and J.X. Tong (2006), "Low temperature firing and microwave dielectric properties of MgTiO₃ ceramics with Bi₂O₃-V₂O₅". *Mater. Lett.*: 60 1188–1191.
- [25] H.K. Shin, H. Shin, H. S. Jung, S.Y. Cho, J.R. Kim, and K. S. Hong (2006), "Role of lithium borosilicate glass in the decomposition of MgTiO₃ based dielectric ceramic during sintering". *Mater. Res. Bull.*: 41 1206–1214.
- [26] H. Jantunen, R. Rautioaho, A. Uusumaki, and S. Leppavuori (2000), "Preparing low loss low temperature cofired ceramic material without glass addition". *J. Am. Ceram. Soc.*: 83 2855–2857.
- [27] H. Jantunen, A. Uusumaki, R. Rautioaho, and S. Leppavuori (2002), "Temperature coefficient of microwave resonance frequency of a low temperature cofired (LTCC) system". *J. Am. Ceram. Soc.*: 85 697–699.

[28] H. Jantunen, A. Uusumaki, R. Rautioaho, and S. Leppavuori (2000), "Compositions of MgTiO₃- CaTiO₃ ceramic with two borosilicate glasses for LTCC technology". J. Eur. Ceram. Soc.: 20 2331–2336.

[29] T. Hu, R. Rautioaho, H. Jantunen, S. Leppavuori, K. Soponmanee, and S. Sirisoonthorn (2005), "Optimisation of MgTiO₃–CaTiO₃ based LTCC tapes containing B₂O₃ for use in microwave applications". Ceram. Int.: 31 85–93.

[30] Y.-J. Choi, J.-H. Park, J.-H. Park, and J.-G. Park (2004), "Middle permittivity LTCC dielectric composition with adjustable temperature coefficient". Mater. Lett.: 58 3102–3106.

[31] G. Kiziltas, D. Psychoudakis, J. L. Volakis and N. Kikuchi (2003), "Topology design optimization of dielectric substrates for bandwidth improvement of a patch antenna," IEEE Transactions on Antennas and Propagation: 51(10) 2732 – 2743.

[32] R.E. Mistler, E.R. Twiname (2000), "Tape Casting Theory and Practice", The American Ceramic Society.

[33] M.D. Bruch and J.A.K. Bonesteel (1986), "Interpretation of the Proton NMR Spectrum of Poly(vinylbutyral) by Two-Dimensional NMR", Macromolecules: 19(6), 1622-1627.

[34] S. Amiya, S. Tsuchiya, R. Qian, A. Nakajima (1990), "The Study of Microstructures of Poly (Vinyl Alcohol) by NMR", Pure Appl. Chem.,: 62 (11) 2139-2146.

[35] Polyvinlyl butyral FT-IR spectrum from website

<http://webbook.nist.gov/cgi/cbook.cgi?ID=C78933&Units=SI&Type=IRSPEC&Index=18#IR-SPEC>

[36] Polyvinlyl butyral FT-IR spectrum from website

<http://webbook.nist.gov/chemistry/name-ser.html>

[37] FT-IR spectrum of Polyethylene glycol Mw. 1500

<http://www.chemexper.com/index.shtml?main=http://www.chemexper.com/search/cas/2432-99-7.html>

7. APPENDIX

Materials Impedance Analyzer Measurement Error Types

1. Gap Error

This error consists of two factors as following: Measurement Error of Test Material's Thickness (Error caused by Micrometer) : Thickness measurement of the test material depends on accuracy of the micrometer used. To reduce this error, measure the thickness at several points of the measured area of the test material using an accurate micrometer. Do not use the micrometer equipped with the 16451B. Parallelism and Flatness of Electrodes and Test Material : When contacting the MUT directly with the electrodes, an airgap is formed between the MUT and the electrodes. No matter how at and parallel both sides of the MUT is fabricated, an airgap will still form. This airgap is the cause for measurement error because the measured capacitance will be the sum of the capacitance of the dielectric material and the airgap. The relationship between the airgap's thickness and measurement error is determined by the equation shown in Figure below. Measurement error is a function of the relative permittivity (ϵ_r') of the MUT, thickness of the MUT (d), and the airgap's thickness (t). Sample results of measurement error have been calculated in Table 1. Notice that the effect is greater with thin materials and materials with high permittivity

This airgap effect can be eliminated, by applying a thin film electrode to the surfaces of the dielectric material. An extra step is required for material preparation (fabricating a thin film electrode), but the most accurate measurements can be performed.

Table 1. Measurement Error caused by Airgap

t/d	$\epsilon_r' = 2$	$\epsilon_r' = 5$	$\epsilon_r' = 10$	$\epsilon_r' = 20$	$\epsilon_r' = 50$	$\epsilon_r' = 100$
0.001	0.1%	0.4%	1%	2%	5%	9%
0.005	0.5%	2%	4%	9%	20%	33%
0.01	1%	4%	8%	16%	33%	50%
0.05	5%	16%	30%	48%	70%	83%
0.1	8%	27%	45%	63%	82%	90%

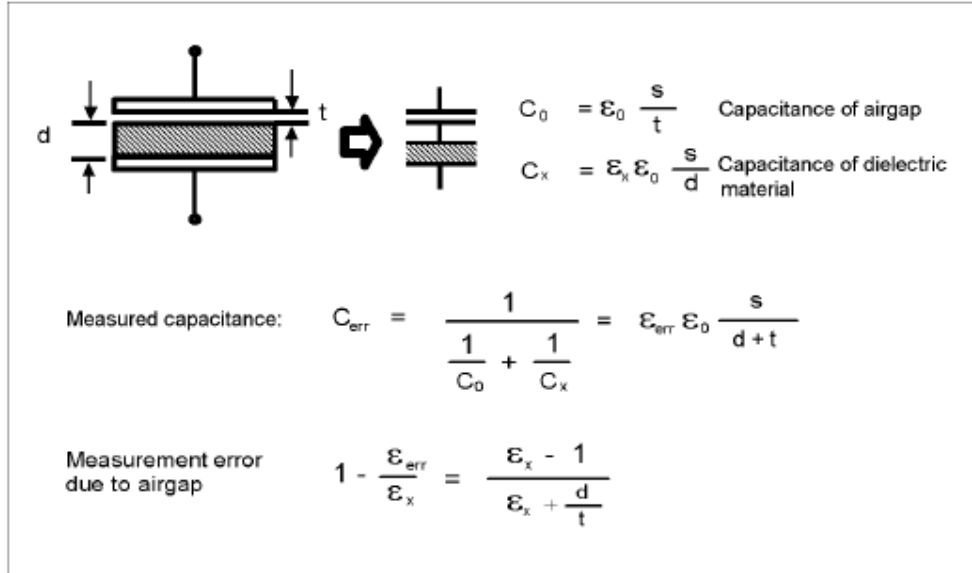


Figure 1. Airgap effects

2. Tolerance of Guarded Electrode Diameter

This error depends on the electrodes mechanical accuracy. The typical error for Electrode-A (-38 mm electrode) and Electrode-B (-5 mm electrode) are given in Table 2, below.

Table.2. Tolerance of Electrode Diameter

Electrode	Tolerance (typical)
Electrode-A ($\phi 38$ mm Electrode)	approximately $\pm 0.13\%$
Electrode-B ($\phi 5$ mm Electrode)	approximately $\pm 1.0\%$

Calculation of the dielectric constant from the capacitance value:

$$\epsilon = \epsilon_0 \epsilon_r$$

$$\epsilon = \frac{t}{A} C_p$$

where;

ϵ : Dielectric constant (permittivity) [F/m]

ϵ_0 : Space Permittivity = 8.854×10^{-12} [F/m]

ϵ_r : Relative Dielectric Constant (Relative permittivity of test material) of test material

C_p : Equivalent Parallel Capacitance Value [F]

t: Thickness of test material [m]